# Analyses of a slender body moving near a curved ground

Q. X. Wang[a)]
*Maritime Research Centre, School of Civil and Environmental Engineering, Nanyang Technological University, 50 Nanyang Avenue, Singapore 630798, Republic of Singapore*

(Received 20 February 2005; accepted 15 July 2005; published online 30 August 2005)

The irrotational flow induced by a slender body moving near a curved ground is analyzed by extending the classical slender body theory. The flow far away from the body is shown to be a direct problem, represented by the line source distribution along the body long axis, whose strength is at the variation rate of the double cross-section areas of the body. The flow near the body is reduced to the two-dimensional flow problem of the deformation, vertical and lateral translations of double cylinders in a symmetrical manner. In particular, an analytical flow solution is obtained for a slender body of revolution at angles of attack and yaw, moving near an arbitrary curved ground. The attraction and side force, and pitching and yaw moments, acting on the body, are obtained in the form of the integrals along the body length by using the control volume method. Numerical analyses are then performed for the body moving near flat, convex, concave, and wavy grounds, respectively. The analyses reveal the orders of the attraction and side force, and pitching and yaw moments, as well as their variation trends in terms of the angles of attack and yaw of the body, the profile of the curved ground, and the clearance between them, etc. These irrotational dynamic features provide a basic understanding of the problem, which will be beneficial to further numerical and experimental studies involving more physical effects. 
[DOI: 10.1063/1.2034867]

## I. INTRODUCTION

The so-called extreme ground effect is for a body moving in very close proximity to a weakly curved ground (or a water surface), where the ratio of the clearance beneath the body to the body length is under 10%. A wing in the extreme ground effect was studied by Widnall and Barrows,[1] Yih,[2] Tuck,[3,4] Newman,[5] and Wang.[6] Those works are based on the potential flow theory and the method of matched asymptotic expansions. It has been proven that, up to the third-order approximation, the flow above the wing is reduced to a direct problem and the flow beneath it appears to be a two-dimensional channel flow. Thus, as indicated by Widnall and Barrows,[1] the extreme-ground-effect theory for wings forms an interesting complement to Prandtl's lifting line theory and Jones's slender body theory. Reviews about the extreme ground effect on wings can be found in Refs. 7 and 8.

There have been only a very few theoretical studies on a body in ground effect based on the potential flow theory. Newman[9] studied a slender body of revolution at zero incidence moving over a flat wall, by representing the flow in terms of a curved line source along the body, together with its image to the flat wall. Tuck and Newman,[10] Yeung and co-workers,[11,12] and Cohen and Beck[13] analyzed two slender bodies far apart using the far-field approximations of the slender body theory, assuming the clearance between them is comparable to their lengths.

In contrast, a slender body in ground effect is of practical importance in a few fields. It has applications for a ship moving near a bank (such as berthing to a quay wall), near another ship, or in shallow water, and a submarine moving close to the seabed. For those cases, the attraction due to ground effect may be comparable to the buoyancy acting on the body, as to be shown in Sec. IV. It also has applications for ground vehicles at very high speeds.[14] As an illustration, the maximum speed of magnetic trains reaches 360 mph. As to be shown in Sec. IV too, the attraction acting on a train at such a high speed due to ground effect may be three orders larger than the air buoyancy on it. The applications exist as well for a missile skimming over a sea surface.

Most of the studies on ground effect concern only a flat ground. But the ground (or water surface) is actually curved in the practical problems. Furthermore, the unsteady effect due to the ground curvature is of the same order as the corresponding flat ground effect, when the undulation amplitude of the curved ground is comparable with the clearance between the body and ground.[6,15,16]

With the above considerations, this work addresses a slender body in extreme curved-ground effect. We assume that the transverse scales and angles of attack and yaw of the body, the amplitude of the ground undulation, and the clearance between them are small quantities of the same order of magnitude. This work is based on the potential flow theory too, since it provides a good approximation for high Reynolds number flows. The flow analysis is carried out by extending the classical slender body theory

A few decades ago, the slender body theory was one of the most popular theorems in aerodynamics as well as in marine hydrodynamics.[17–21] Such a success was, in part, because of the poor computational abilities of that time. Nowadays, the powerful modern computational capabilities allow us to compute the flow around bodies of arbitrary form. Nev-

[a)]Electronic mail: cqxwang@ntu.edu.sg

 

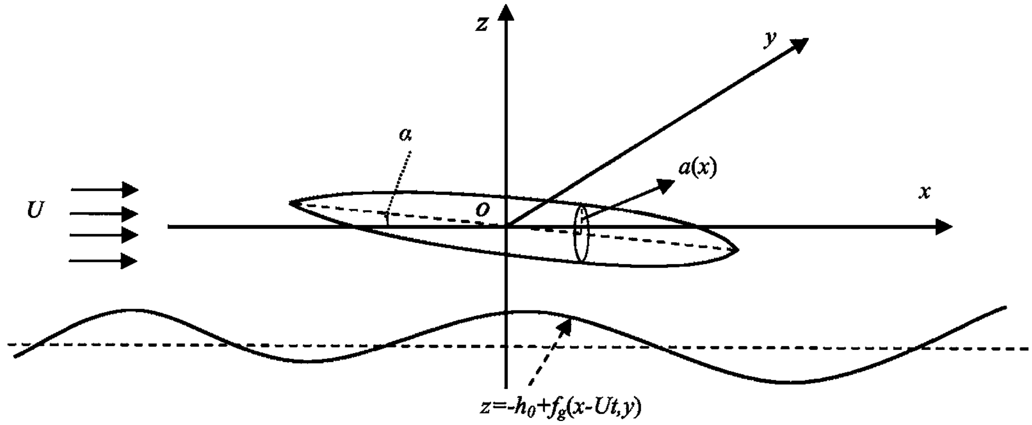


FIG. 1. A slender body in a horizontal translation in very close proximity to a curved ground.

ertheless, it remains highly desirable to be able to predict, and to explain, at reasonable time cost, the main features of a flow around a body; clearly the numerical way does not provide the whole answer. Hence, in the case of a slender body in extreme ground effect, a formal and asymptotic perturbation theory remains quite useful.

The remainder of the paper is organized as follows. In Sec. II, the flow problem of a slender body in curved-ground effect is analyzed using the method of matched asymptotic expansions. In Sec. III, an analytical flow solution is obtained for a slender body of revolution at angles of attack and yaw in curved-ground effect using the conformal mapping. The formulas for the force and moment on the body are obtained in Sec. IV using the control volume method. Section V performs the numerical analyses for the body moving over flat, convex, concave, and wavy grounds, respectively. Section VI contains the summary and conclusions of this work.

## II. FLOW ANALYSIS OF SLENDER BODY IN CURVED-GROUND EFFECT

### A. Mathematical modeling

Consider a slender body at angles of attack $\alpha^*$ and yaw $\delta^*$, translating horizontally in close proximity to a weakly curved ground of infinite extent, as shown in Fig. 1. A Cartesian coordinate system $O$-$xyz$ fixed to the body is defined, with the origin located at the center point of its long axis, $x$ axis along the flow direction at infinity and $z$ axis pointing upwards. Denote the body length as $L$ and the body horizontal velocity as $U$. The slender body can be represented as

$$r_2 = a(x,\theta) \quad \text{for } 0 \leqslant \theta \leqslant 2\pi \text{ and } |x| \leqslant L/2, \tag{1}$$

where

$$r_2 = \sqrt{(y-\delta^* x)^2 + (z+\alpha^* x)^2}, \quad \theta = \arctan\left(\frac{z+\alpha^* x}{y-\delta^* x}\right), \tag{2}$$

and $a(r,\theta)$ is the radius distribution of the cross section of the body, which is required to be a smooth function, to be vanished at the nose and to vary slowly along the body.

The curved ground can be expressed as

$$z = -h_0 + f_g(x-Ut,y), \tag{3}$$

where $h_0$ is the elevation of the body center above the mean plane of the curved ground.

Following the geometrical assumption outlined in Sec. I, it is assumed that

$$a(x,\theta), \alpha^*, \delta^*, h_0, f_g(x-Ut,y) = O(\varepsilon), \tag{4a}$$

where $\epsilon$ is the ratio of the maximum radius of the cross section of the body to the length of the body. We therefore can express those parameters as

$$a(x,\theta) = \varepsilon A(x,\theta),$$

$$\alpha^* = \varepsilon\alpha, \quad \delta^* = \varepsilon\delta, \quad h_0 = \varepsilon H_0,$$

$$f_g(x-Ut,y) = \varepsilon F_g(x-Ut,y), \tag{4b}$$

where

$$A(x,\theta), \alpha, \delta, H_0, F_g(x-Ut,y) = O(1). \tag{4c}$$

We further assume that the fluid is inviscid and incompressible and that the flow is irrotational. A disturbance velocity potential $\varphi(x,y,z,t)$ exists in the fluid domain bounded by the body and ground, and satisfies the Laplace equation in the fluid domain,

$$\varphi_{xx} + \varphi_{yy} + \varphi_{zz} = 0, \tag{5a}$$

subjected to suitable boundary conditions. $\varphi$ is required to vanish at infinity. The impermeable boundary condition on the body surface is

$$\varphi_n \sqrt{1+\left(\frac{a_\theta}{a}\right)^2} = -U\left[a_x + \delta^* \cos\theta - \alpha^* \sin\theta + \frac{a_\theta}{a}(\delta^* \sin\theta + \alpha^* \cos\theta)\right] + O(\varepsilon\varphi), \tag{5b}$$

where $\boldsymbol{n}$ is the unit outward normal vector of the fluid domain on the body surface.

The impermeable boundary condition on the curved ground is

$$\varphi_z = f_{gx}\varphi_x + f_{gy}\varphi_y \quad \text{on } z = -h_0 + f_g(x - Ut, y). \tag{5c}$$

As an illustration, we discuss the physical assumptions for typical marine vessels and high-speed trains, which are usually streamlined slender bodies. The Reynolds numbers $R_e$ of those flow problems in terms of the body length are at the order of $O(10^8)$ or larger, and consequently thin turbulent boundary layers surround the bodies. Since the body is with small angles of attack and yaw and a gradual change of radius, there should be no significant boundary layer separation. The maximum displacement thickness of the boundary layer can be estimated as $\delta_d = 0.046LR_e^{-0.2} \leqslant 1 \times 10^{-3}L$ (cf. Ref. 22). The potential flow model is thus suitable when the minimum clearance $C_{\min}$ between the body and wall is one order larger than $\delta_d$, i.e., $C_{\min} \geqslant 1 \times 10^{-2}L$. In addition, the condition on the minimum clearance may be violated locally without destroying the validity of the potential flow solution as a whole.[23] When the boundary layer thickness is comparable to the clearance, the viscous and inertial forces are comparable in the flow field beneath the body.[24]

### B. Outer expansion

In the outer region far away from the body, $x, y, z = O(1)$, where the boundary condition on the ground surface (5c) becomes

$$\varphi_z = O(\varepsilon\varphi) \quad \text{on } z = O(\varepsilon). \tag{6}$$

To the first-order approximation, the curved ground can thus be regarded as a plane wall with no flux boundary condition for the outer expansion. Using the image method, the flow disturbance in the outer region can be regarded as the repellence of the fluid due to the body and its reflected image to the plane wall $z=0$. Both the slender body and its image shrink to the line segment, $|x| \leqslant L/2$ and $y=z=0$, as seen by an outer observer. In fact, the flux per unit length of the body is specified and the no flux boundary condition on the ground implies that the resulting disturbance must be found in the half space instead of a full space. It is therefore inferred that the outer expansion $\varphi^o$ can be expressed in terms of the line source along the segment

$$\varphi^o(x,y,z,t) = \varepsilon^2 \int_{-L/2}^{L/2} \frac{F(\xi)d\xi}{\sqrt{(x-\xi)^2 + y^2 + z^2}} + o(\varepsilon^2), \tag{7}$$

where $4\pi F(\xi)$ is the strength of the line source. The above equation can be derived from the Green formula for $\varphi^o$ since the contribution of the doublet distribution in the far field is one order smaller than that of the source distribution. $F(\xi)$ will be determined in Sec. II D as the variation rate of the double cross-section areas of the slender body,

$$F(x) = \frac{U}{2\pi}\frac{d}{dx}\left[\int_0^{2\pi} \frac{A^2(x,\theta)}{2} d\theta\right]. \tag{8}$$

The velocity potential in the outer region is thus steady, axisymmetric, and is equal to the flow around a slender body of revolution at the double cross-section areas in an unbounded fluid. In particular, for a slender body of revolution,

$$F(x) = UA(x)A_x(x). \tag{9}$$

### C. Inner expansion

We next consider the flow in the inner region, where $x = O(1)$ and $y$, $z = O(\epsilon)$. Introduce the inner variables

$$x = x, \quad Y = (y - \delta^* x)/\varepsilon, \quad Z = (z + \alpha^* x)/\varepsilon. \tag{10}$$

The inner limit of the outer expansion $\varphi^o$ can obtained from (7)

$$(\varphi^o)^i = \varepsilon^2 G(x) - 2\varepsilon^2 \ln \varepsilon F(x) - \varepsilon^2 F(x)\ln(Y^2 + Z^2) + o(\varepsilon^2), \tag{11a}$$

where

$$G(x) = \int_{-L/2}^{L/2} F_\xi(\xi)\ln|2\xi - 2x| d\xi. \tag{11b}$$

The inner expansion of the velocity potential can be conjectured from the inner limit of the outer expansion of (11a)

$$\varphi^i = \varepsilon^2 G(x) - 2\varepsilon^2 \ln \varepsilon F(x) + \varepsilon^2 \phi(x,Y,Z,t) + o(\varepsilon^2), \tag{12}$$

where $\phi$ satisfies the Neumann boundary-value problem of the two-dimensional Laplace equation in a triply connected domain in the cross-flow plane, obtained from (5) and (12)

$$\phi_{YY} + \phi_{ZZ} = 0, \tag{13a}$$

$$\phi_n \sqrt{1 + \left(\frac{A_\theta}{A}\right)^2} = -U\left[A_x + \delta\cos\theta - \alpha\sin\theta + \frac{A_\theta}{A}(\delta\sin\theta + \alpha\cos\theta)\right] \quad \text{on } R_2 = A(x,\theta), \tag{13b}$$

$$\phi_Z = 0 \quad \text{on } Z = -H(x,t), \tag{13c}$$

where

$$R_2 = \sqrt{Y^2 + Z^2}, \quad \theta = \arctan(Z/Y),$$

$$H(x,t) = H_0 - \alpha x - F_g(x - Ut, 0). \tag{14}$$

Using the image method and examining (13), one can see that the flow near the body is reduced to the two-dimensional flow problem of the deformation, the vertical and lateral translations of double cylinders, in a symmetrical manner. The influence of the deformation, corresponding to the variation of the cross-section shape of the body, propagates to the outer region; whereas other influences are limited in the inner region. The three problems cannot be decoupled as that for a slender body in an unbounded fluid. The unsteady effect of the ground curvature depends only on the ground undulation along the body length, and is limited in the inner region. Note that the kinematic features observed above are limited to the first-order approximation.

### D. Matching of inner and outer expansions

Because $\phi$ satisfies the two-dimensional Laplace equation (13a) and zero flux boundary condition (13c) on $Z = -H$, $\phi$ can be expressed as follows using the Green formula:

$$\phi(x,Y,Z,t) = \oint_{C_1} \left[ G(Y,Z,Y_0,Z_0) \frac{\partial \phi(x,Y_0,Z_0,t)}{\partial n} - \frac{\partial G(Y,Z,Y_0,Z_0)}{\partial n} \phi(x,Y_0,Z_0,t) \right] dl(Y_0,Z_0). \tag{15}$$

Note that the integral is carried out only on the periphery $C_1$ of the cross section of the body, since the boundary condition on ground (13c) has been taken into account in the Green function $G(Y,Z,Y_0,Z_0)$,

$$G(Y,Z,Y_0,Z_0) = \frac{1}{2\pi} \ln\{[(Y-Y_0)^2 + (Z-Z_0)^2][(Y-Y_0)^2 + (Z-Z_0+2H)^2]\}. \tag{16}$$

As $R_2 = \sqrt{Y^2+Z^2} \to \infty$, (15) becomes

$$\phi(x,Y,Z,t) = \frac{1}{\pi} \ln R_2 \oint_{C_1} \frac{\partial \phi(x,Y_0,Z_0,t)}{\partial n} dl(Y_0,Z_0) + O(R_2^{-1}). \tag{17}$$

Substituting normal derivative $\phi_n$ of (13b) into (17) and using

$$\int_0^{2\pi} \left[ \delta \cos\theta - \alpha \sin\theta + \frac{A_\theta}{A}(\delta \sin\theta + \alpha \cos\theta) \right] A d\theta = \int_0^{2\pi} \frac{d}{d\theta}[A(\delta \sin\theta + \alpha\cos\theta)] d\theta \equiv 0, \tag{18}$$

the outer limit of $\phi$ is obtained as

$$\phi = -\frac{U}{\pi} \ln R_2 \frac{d}{dx} \oint \frac{A^2(x,\theta)}{2} d\theta + O(R_2^{-1}). \tag{19}$$

The matching condition (8) can be obtained by equating the inner limit of the outer expansion (11a) to the outer limit of the inner expansion (12) and (19), according to Van Dyke's matching principle.[23]

## III. ANALYTIC FLOW SOLUTIONS FOR SLENDER BODY OF REVOLUTION

We consider a special case in this section where a slender body of revolution moves near a curved ground. The cross-flow boundary-value problem of $\phi$ (13) is simplified as

$$\phi_{YY} + \phi_{ZZ} = 0, \tag{20a}$$

$$\phi_R = U(A_x + \delta\cos\theta - \alpha\sin\theta) \quad \text{on } R_2 = A(x), \tag{20b}$$

$$\phi_Z = 0 \quad \text{on } Z = -H(x,t), \qquad H(x,t) = H_0 - \alpha x - F_g(x-Ut,0). \tag{20c}$$

$\phi$ thus can be regarded as the two-dimensional velocity potential induced by the double circular cylinders at the radii $A(x)$, expanding (contracting) at the velocity $UA_x(x)$, approaching each other at the velocity $U\alpha$, and moving perpendicular to the line connecting their centers at the velocity $U\delta$. Wang[25] obtained the velocity potential for two arbitrary moving circular cylinders. For completeness, the solution of (20) is briefed as follows.

To solve the problem of (20), a linear fractional conformal mapping is introduced between the cross-flow plane of $T = Y + iZ$ and the mapped plane of $\varsigma = \rho e^{i\Theta}$,

$$T = iC\frac{\varsigma + C}{\varsigma - C} - iC \coth\beta, \tag{21}$$

where

$$C = \sqrt{H^2 - A}, \quad \beta = \text{arcsinh}(C/A). \tag{22}$$

It maps the domain outside two circles $C_1$, $|T| = A$, and $C_2$, $|T - 2Hi| = A$, in the cross-flow plane $T$ to the domain between the two concentric circles $B_1$, $|\varsigma| = \rho_1$, and $B_2$, $|\varsigma| = \rho_2$, in the mapped plane $\zeta$, as sketched in Fig. 2. $\rho_1$ and $\rho_2$ are

$$\rho_1 = Ce^{\beta}, \quad \rho_2 = Ce^{-\beta}. \tag{23}$$

Note that $C_2$ is the image of $C_1$ to the ground $Z = -H$. The mapping also transforms the line $C_g$, $Z = -H$, in the cross-flow plane $T$ to the circle $B_0$, $|\varsigma| = C$, in the mapped plane $\zeta$.

To simplify the problem of (20), we then introduce

$$\phi = F \ln\rho - 2F \ln|\varsigma - C| + \Phi. \tag{24}$$

The boundary problem of $\Phi$ becomes

$$\Phi_{\rho\rho} + \frac{1}{\rho^2}\Phi_{\Theta\Theta} = 0, \tag{25a}$$

$$\frac{\partial \Phi}{\partial \rho} = U[\alpha f_1(\Theta) - \delta f_2(\Theta)] \quad \text{on } B_1, \tag{25b}$$

$$\frac{\partial \Phi}{\partial \rho} = U\beta^2[\alpha f_1(\Theta) + \delta f_2(\Theta)] \quad \text{on } B_2, \tag{25c}$$

where $f_1(\Theta)$ and $f_2(\Theta)$ can be obtained from (20)–(24),

$$f_1(\Theta = 2\sinh\beta \left[ \frac{\coth\beta}{e^{2\beta} - 2e^{\beta}\cos\Theta + 1} - \frac{e^{2\beta} - 1}{(e^{2\beta} - 2e^{\beta}\cos\Theta + 1)^2} \right], \tag{26a}$$

$$f_2(\Theta) = \frac{4\sinh\beta\sin\Theta}{(e^{2\beta} - 2e^{\beta}\cos\Theta + 1)^2}. \tag{26b}$$

$f_1(\Theta)$ and $f_2(\Theta)$ can be expanded in the Fourier series in $\Theta$ as follows:

$$f_1(\Theta) = -\sum_{n=1}^{\infty} n \frac{\cos(n\Theta)}{e^{(n+1)\beta}}, \tag{27a}$$

$$f_2(\Theta) = 2\sum_{n=1}^{\infty} n \frac{\sin(n\Theta)}{e^{(n+1)\beta}} \tag{27b}$$

by using the following integral formulas:

$$\int_0^{2\pi} \frac{\cos n\Theta \, d\Theta}{a^2 - 2a\cos\Theta + 1} = \frac{2\pi}{a^n(a^2-1)} \quad \text{for } a > 1, \tag{28a}$$

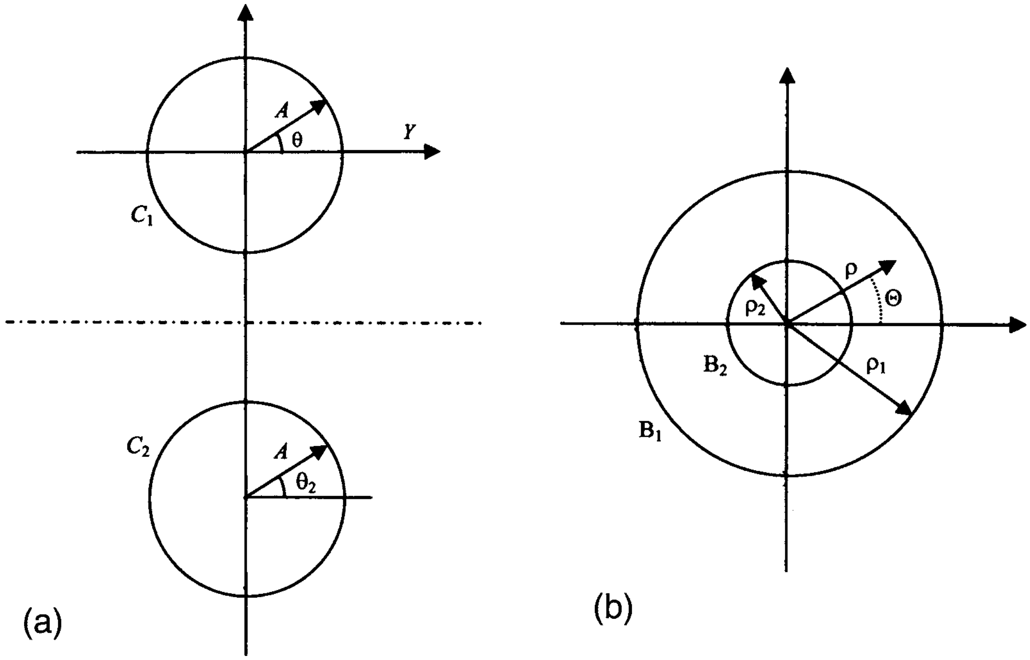


FIG. 2. The conformal mapping of (a) the domain outside two circles $C_1$ and $C_2$, in the cross-flow plane $T=Y+iZ$, to (b) the domain between two concentric circles $B_1$ and $B_2$, in the mapped plane $\zeta=\rho e^{i\Theta}$.

$$\int_0^{2\pi}\frac{\cos n\Theta\, d\Theta}{(a^2-2a\cos\Theta+1)^2} = \frac{2\pi}{a^n(a^2-1)^3}[2+(n+1)(a^2-1)] \quad \text{for } a>1. \tag{28b}$$

We further assume that the solution of (25) takes the form

$$\Phi=\sum_{n=1}^{\infty}(C_n^1\rho^n+C_n^2\rho^{-n})\cos(n\Theta) + \sum_{n=1}^{\infty}(C_n^3\rho^n+C_n^4\rho^{-n})\sin(n\Theta). \tag{29}$$

Determining the coefficients $C_n^i$, $i=1,2,3,4$, in (29) with the boundary conditions (25b), (25c), and (27) and then substituting (29) into (24), we obtain

$$\phi=F\ln\left(\frac{\rho}{\rho^2-2\rho\cos\Theta+C^2}\right) + UC\sum_{n=1}^{\infty}\frac{1}{\sinh(n\beta)}\left[\left(\frac{\rho}{\rho_1}\right)^n+\left(\frac{\rho_2}{\rho}\right)^n\right][\alpha\cos(n\Theta) - \delta\sin(n\Theta)]. \tag{30}$$

The series in (30) is absolutely convergent in the whole cross-flow domain corresponding to $\rho_2\leqslant\rho\leqslant\rho_1$ and $0\leqslant\Theta<2\pi$.

## IV. FORMULAS FOR FORCE AND MOMENT

### A. Slender body

The hydrodynamic force $\boldsymbol{f}$ and moment $\boldsymbol{m}_0$ acting on a body moving in a potential flow can be expressed as follows, by using the control volume approach (cf. Appendix A):

$$\frac{\boldsymbol{f}}{\rho_f}=-\frac{d}{dt}\int_{S_b}\varphi\boldsymbol{n}dS-\int_{S_c}\left(\varphi_n\nabla\varphi-\boldsymbol{n}\frac{1}{2}\nabla\varphi\cdot\nabla\varphi\right)dS, \tag{31a}$$

$$\frac{\boldsymbol{m}_0}{\rho_f}=-\frac{d}{dt}\int_{S_b}\varphi(\boldsymbol{R}_0\times\boldsymbol{n})dS - \int_{S_c}\boldsymbol{R}_0\times\left(\varphi_n\nabla\varphi-\boldsymbol{n}\frac{1}{2}\nabla\varphi\cdot\nabla\varphi\right)dS, \tag{31b}$$

where $S_b$ is the body surface, $S_c$ is a fixed control surface exterior to $S_b$, and $\boldsymbol{n}$ is the unit outward normal vector of the control volume on the control surfaces, as shown in Fig. 3. "$d/dt$" is the material time derivative. $\boldsymbol{m}_0$ is the moment to the initial body center at $t=0$, and $\boldsymbol{R}_0$ is the vector of a point on the control surfaces from the initial body center.

$S_c$ is chosen consisting of the fixed ground $S_g$ and the upper half of a large spherical surface $S_\infty$ in the far field, cut by each other, as shown in Fig. 4. The asymptotic behaviors of $\varphi$ in the far field can be estimated from (7) and (8),

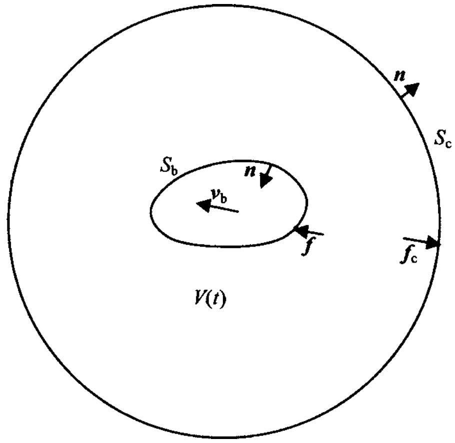


FIG. 3. The control volume $V(t)$ enclosed between a moving body surface $S_b$ and a fixed control surface $S_c$ exterior to $S_b$.

$$\varphi \to O\left(\frac{1}{r^2}\right), \quad |\nabla\varphi| \to O\left(\frac{1}{r^3}\right),$$
$$\varphi_n \to O\left(\frac{1}{r^3}\right) \quad \text{as } r=\sqrt{x^2+y^2+z^2} \to \infty. \tag{32}$$

Since the surface area of $S_\infty$ is proportional to $r^2$, the contribution to the second integrals in (31a) and (31b) from $S_\infty$ will be of order $r^{-4}$ and $r^{-3}$, respectively, and will vanish as $r$ tends to infinity. Noticing further that $\varphi_n=0$ on the ground $S_g$, we obtain

$$\frac{\boldsymbol{f}}{\rho_f} = -\frac{d}{dt}\int_{S_b} \varphi \boldsymbol{n} dS + \frac{1}{2}\int_{S_g} (\nabla\varphi\cdot\nabla\varphi)\boldsymbol{n} dS. \tag{33}$$

One can obtain D'Alembert's paradox for a body moving in ground effect from (33). In fact, for a body in a steady horizontal translation near a plane wall, the first integral in (33) does not depend on time, and the second integral is nonzero only in the vertical direction, hence no drag and side forces act on the body.

For a slender body in curved-ground effect, using the slenderness assumption and inner expansion of (12) and (33) can be simplified as

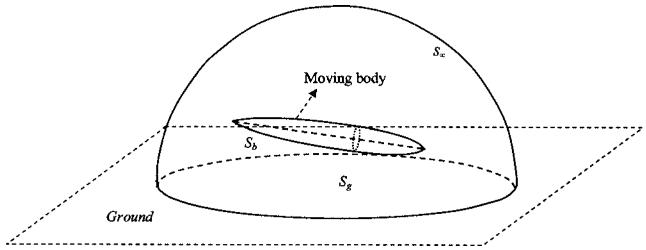


FIG. 4. The control volume, for a slender body moving near a wall, surrounded by the body surface $S_b$, ground $S_g$, and the upper half of a large sphere surface $S_\infty$ in the far field.

$$\frac{\boldsymbol{f}}{\rho_f\varepsilon^3} = -\frac{d}{dt}\int_{-L/2}^{L/2} dx \oint_{C_1} \phi \boldsymbol{n} dl - \frac{\boldsymbol{k}}{2}\int_{-L/2}^{L/2} dx \int_{C_g} (\phi_Y^2+\phi_Z^2) dl + O(\varepsilon), \tag{34}$$

where $\boldsymbol{k}$ is the unit vector along the $z$ axis.

Introducing $I_1(x,t)$, $J_1(x,t)$, and $J_2(x,t)$, as follows:

$$I_1(x,t) = \oint_{C_1} \phi\cos\theta\, dl, \tag{35a}$$

$$J_1(x,t) = \oint_{C_1} \phi\sin\theta\, dl, \tag{35b}$$

$$J_2(x,t) = \frac{1}{2}\oint_{C_g} (\phi_Y^2+\phi_Z^2) dl, \tag{35c}$$

the side force $f_y$ and vertical force $f_z$ can be given as follows from (34):

$$\frac{f_y}{\rho_f\varepsilon^3} = \int_{-L/2}^{L/2} I_{1t}(x,t) dx + O(\varepsilon), \tag{36a}$$

$$\frac{f_z}{\rho_f\varepsilon^3} = \int_{-L/2}^{L/2} [J_{1t}(x,t) - J_2(x,t)] dx + O(\varepsilon). \tag{36b}$$

In the similar way, using the slenderness assumption, (31b) can be simplified as

$$\frac{\boldsymbol{m}_0}{\rho_f\varepsilon^3} = -\frac{d}{dt}\int_{-L/2}^{L/2} dx \oint_{C_1} \phi \boldsymbol{R}_0 \times \boldsymbol{n} dl - \frac{1}{2}\int_{-L/2}^{L/2} \boldsymbol{R}_0 \times \boldsymbol{k} dx \times \int_{C_g} (\phi_Y^2+\phi_Z^2) dl + O(\varepsilon), \tag{37}$$

where

$$\boldsymbol{R}_0 = (x-Ut)\boldsymbol{i} + y\boldsymbol{j} + z\boldsymbol{k} = (x-Ut)\boldsymbol{i} + O(\varepsilon), \tag{38a}$$

$$\boldsymbol{n} = \cos\theta\,\boldsymbol{j} + \sin\theta\,\boldsymbol{k} + O(\varepsilon), \tag{38b}$$

where $\boldsymbol{i}$ and $\boldsymbol{j}$ are the unit vectors along $x$ and $y$ axes.

Substituting (38) into (37),

$$\begin{aligned}\frac{\boldsymbol{m}_0}{\rho_f\varepsilon^3} &= \frac{d}{dt}\int_{-L/2}^{L/2} (x-Ut) dx \oint_{C_1} \phi(\cos\theta\,\boldsymbol{k} - \sin\theta\,\boldsymbol{j}) dl \\ &\quad + \boldsymbol{j}\frac{1}{2}\int_{-L/2}^{L/2} (x-Ut) dx \int_{C_g} (\phi_Y^2+\phi_Z^2) dl + O(\varepsilon) \\ &= \frac{d}{dt}\int_{-L/2}^{L/2} (x-Ut)(I_1\boldsymbol{k} - J_1\boldsymbol{j}) dx \\ &\quad + \boldsymbol{j}\int_{-L/2}^{L/2} (x-Ut) J_2 dx + O(\varepsilon) \\ &= -Ut\int_{-L/2}^{L/2} [I_{1t}\boldsymbol{k} + (J_2 - J_{1t})\boldsymbol{j}] dx\end{aligned}$$

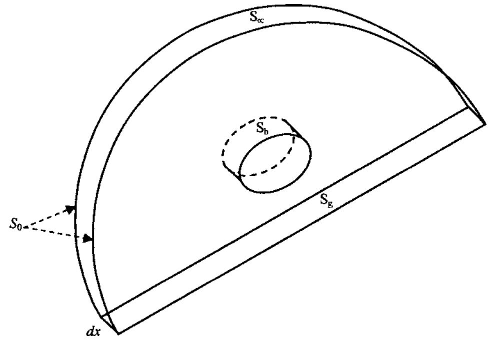


FIG. 5. The control volume for the evaluation of the differential force $\boldsymbol{df}$ on a cross section of a slender body moving over ground.

$$+\int_{-L/2}^{L/2}[(UJ_1 - xJ_{1t} + xJ_2)\boldsymbol{j} + (-UI_1 + xI_{1t})\boldsymbol{k}]dx + O(\varepsilon). \quad (39)$$

Considering that the body moves at the velocity $-U\boldsymbol{i}$, the pitching moment $m_y$ to the $y$ axis and the yaw moment $m_z$ to the $z$ axis can be given as

$$\frac{m_y}{\rho_f\varepsilon^3} = \int_{-L/2}^{L/2}[UJ_1(x,t) - xJ_{1t}(x,t) + xJ_2(x,t)]dx + O(\varepsilon), \quad (40a)$$

$$\frac{m_z}{\rho_f\varepsilon^3} = \int_{-L/2}^{L/2}[-UI_1(x,t) + xI_{1t}(x,t)]dx + O(\varepsilon). \quad (40b)$$

To calculate the differential lateral force $\boldsymbol{df}$ along the body length, (31a) is applied to a thin slice of fluid of differential thickness $dx$, as shown in Fig. 5. Here $S_b$ in (31a) is chosen as the differential length of the body surface. $S_c$ consists the differential length of the ground surface $dS_g$, the two lateral planes $S_0$ separated by a distance of $dx$ external to the body and above the ground, and a closure surface $dS_\infty$ at a large radial distance from the body.

The contributions to the second integration of (31a) from the two lateral planes $S_0$ are

$$E_y = -\frac{\partial}{\partial x}\int_{S_0}\frac{\partial\varphi}{\partial x}\frac{\partial\varphi}{\partial y}dS, \quad E_z = -\frac{\partial}{\partial x}\int_{S_0}\frac{\partial\varphi}{\partial x}\frac{\partial\varphi}{\partial z}dS. \quad (41)$$

To estimate $E_y$ and $E_z$, $S_0$ is divided into two parts: $S_{01}$, where $r=o(1)$ with the area $A_1=o(1)$, and $S_{02}$, where $r \geqslant O(1)$ with the area $A_2=O(r^2)$. Using the slenderness assumption, we have

$$\varphi_x = O(\varepsilon^2), \quad \varphi_y = O(\varepsilon), \quad \varphi_z = O(\varepsilon) \quad \text{on } S_{01}. \quad (42a)$$

Using (7) and (8), we know

$$\varphi_x = O(\varepsilon^2/r^3), \quad \varphi_y = O(\varepsilon^2/r^3), \quad \varphi_z = O(\varepsilon^2/r^3) \quad \text{on } S_{02}. \quad (42b)$$

With the above estimations, one can obtain $E_y$, $E_z=o(\varepsilon^3)$.

Similar to the derivation of (36), and considering the contribution from the two lateral planes $S_0$ canceled, one can obtain the differential force components $df_y$ and $df_z$,

$$\frac{df_y}{\rho_f\varepsilon^3} = \frac{dI_1(x,t)}{dt} + o(1), \quad (43a)$$

$$\frac{df_z}{\rho_f\varepsilon^3} = \frac{dJ_1(x,t)}{dt} - J_2(x,t) + o(1). \quad (43b)$$

Note here that Lighthill[19] used the above approach to calculate the differential lateral force in analyzing the swimming motion of slender fish.

## B. Slender body of revolution

The three integrals in (35) can be integrated analytically for a slender body of revolution (cf. Appendix B)

$$I_1(x,t) = -4\pi C^2 U\delta\sum_{n=1}^{\infty}[n\coth(n\beta)e^{-2n\beta}], \quad (44a)$$

$$J_1(x,t) = 2\pi F(H-C) + 4\pi C^2 U\alpha\sum_{n=1}^{\infty}[n\coth(n\beta)e^{-2n\beta}], \quad (44b)$$

$$J_2(x,t) = \frac{\pi}{C}\left[F^2 + 2AFU\alpha e^{-\beta} + 2C^2U^2(\alpha^2+\delta^2)\sum_{n=1}^{\infty}c_n(c_n - c_{n+1})\right], \quad (44c)$$

where

$$c_n = \frac{2ne^{-2n\beta}}{1-e^{-2n\beta}}. \quad (45)$$

$I_{1t}$, $J_{1t}$ needed in (36) and (40) can be obtained from (44a) and (44b) as follows:

$$I_{1t}(x,t) = -4\pi CU\delta\sum_{n=1}^{\infty}d_n e^{-2n\beta}, \quad (46a)$$

$$J_{1t}(x,t) = 2\pi F(H_t - C_t) - 8\pi CU\alpha\sum_{n=1}^{\infty}d_n e^{-2n\beta}, \quad (46b)$$

where

$$d_n = n[2(C_t - nC\beta_t)\coth(n\beta) - nC\beta_t\,\mathrm{csch}^2(n\beta)]. \quad (47)$$

$C_t$, $H_t$, and $\beta_t$ needed in (46) and (47) can be obtained from (20c) and (22),

$$H_t = UF_{gx}, \quad C_t = \frac{HH_t}{C}, \quad \beta_t = \frac{C_t}{A\cosh\beta}. \quad (48)$$

The three series in (44) and (46) are convergent absolutely.

Noticing from (44)–(46), $I_1(x,t)$, and $I_{1t}(x,t)$ are linear to $\delta$, $J_1(x,t)$ and $J_{1t}(x,t)$ do not depend on $\delta$, and $J_2(x,t)$ is proportional to $\delta^2$. Noticing further from (36) and (40), the side force and yaw moment are proportional to the angle of yaw, whereas the vertical force and pitching moment are proportional to the square of the angle of yaw.

At zero angles of attack and yaw, the attraction and pitching moment are

$$f_z = -\pi\varepsilon^3\rho_f U^2 \int_{-L/2}^{L/2} \left(\frac{F^2}{C} + 2U\frac{H-C}{C}FF_{gx}\right)dx + O(\varepsilon^4), \tag{49a}$$

$$m_y = \pi\varepsilon^3\rho_f U^2 \int_{-L/2}^{L/2} \left[\frac{F^2}{C}x + 2U\frac{H-C}{C}FF_{gx}x + 2UF(H-C)\right]dx + O(\varepsilon^4). \tag{49b}$$

If the ground is flat, (49) can be further simplified as

$$f_z = -\pi\varepsilon^3\rho_f U^2 \int_{-L/2}^{L/2} \frac{(AA_x)^2}{\sqrt{H_0^2 - A^2}}dx + O(\varepsilon^4), \tag{50a}$$

$$m_y = \pi\varepsilon^3\rho_f U^2 \int_{-L/2}^{L/2} \left[\frac{x(AA_x)^2}{\sqrt{H_0^2 - A^2}} + 2AA_x(H_0 - \sqrt{H_0^2 - A^2})\right]dx + \mathrm{O}(\varepsilon^4). \tag{50b}$$

$f_z$ in (50a) is the same as that obtained by Newman.[9]

For a slender spheroid,

$$a(x) = \varepsilon\sqrt{1 - 4(x/L)^2}, \quad \text{for } |x| \leq L/2. \tag{51}$$

$f_z$ in (50) can be integrated analytically,

$$f_z = -\pi\varepsilon^3\rho_f U^2 L^2 \left[2H_0 + (H_0^2 - 1)\log\left(\frac{H_0 - 1}{H_0 + 1}\right)\right]. \tag{52}$$

The attraction reaches its maximum of $2\pi\varepsilon^3\rho_f U^2 L^2$ at $H_0 = 1$ when the lowest point of the body slides on the wall. Taking $\varepsilon = 0.1$, the maximum attraction is equal to 0.1, 1.0, 10, 100, and 1000 times of the buoyancy on the body at $U = 1.8$, 5.7, 18, 57, and 180 m/s, respectively.

Before ending this section, we discuss the situation when the lowest point of the body slides on the wall. The parts of the integrants containing $(H_0^2 - A^2)^{-1/2}$ in (50a) and (50b) are singular at the contact point, but the integrals are convergent. In fact, near the contact point $x = x_0$,

$$A^2(x) = H_0^2 + 2AA_x(x - x_0) + O[(x - x_0)^2], \tag{53}$$

As an illustration, the integrand of (50a) is

$$\frac{(AA_x)^2}{\sqrt{H_0^2 - A^2}} = \frac{(AA_x)^2}{\sqrt{2AA_x(x - x_0) + O[(x - x_0)^2]}}. \tag{54}$$

The integral of (50a) is thus convergent. The above analysis is for the case of zero incidence. As for cases at an angle of attack, it has been noticed too in the simulations of Sec. V that the integrals in (36) and (40) are convergent numerically, when the body slides on the wall.

In real applications, the viscous effects are significant near the contact point since the clearance beneath the body is smaller than the thickness of the boundary layer over there. As a result, the velocity, pressure, and stress are finite near the impact point. The hydrodynamic load exerted over the small region near contact is at the order of the area of the region, and is small as compared to the global force. The potential flow theory still holds globally when the contact happens locally.

## V. NUMERICAL EVALUATION

The force and moment on a slender body of revolution in ground effect, modeled in Sec. IV, are calculated using MATLAB. The three series in (44) and (46), with their terms decaying exponentially, converge rapidly. The series are summed at a very high accuracy, with the series truncated when the terms are at $O(10^{-10})$ since the CPU time needed is minimal. The components of the force and moment of (36) and (40) are integrated using the recursive adaptive Simpson quadrature, with the error limit set at $10^{-7}$. The calculation results are given in dimensionless parameters defined as follows:

$$F_y = \frac{f_y}{\rho_f U^2 L^2 \varepsilon^3}, \quad F_z = \frac{f_z}{\rho_f U^2 L^2 \varepsilon^3}, \tag{55a}$$

$$M_y = \frac{m_y}{\rho_f U^2 L^3 \varepsilon^3}, \quad M_z = \frac{m_z}{\rho_f U^2 L^3 \varepsilon^3}. \tag{55b}$$

### A. Flat-ground effect

We first consider the case where a slender spheroid moves over a plane wall, a steady problem. Figure 6(a) shows the attraction $-F_z$ on the body versus its center height $H_0$ at the angles of attack $\alpha = 0.0$, 1.0, 1.5, and 2.0, respectively. Attraction acts on the body as expected, because the flow moves faster and the pressure is thus lower beneath the body than those above it, due to the constraining effect of the wall. When the minimum clearance beneath the body is within the radius of the ellipsoid, $H_0 < 2.0$, the attraction is prominent and increases rapidly with decreasing $H_0$. The attraction increases with the angle of attack too. Each curve in Fig. 6(a) starts at the minimum value of $H_0$, at which the lowest point of the body is sliding on the wall. One can see that the attraction reaches its maximum value of $2\pi$ at $\alpha = 0.0$ and $H_0 = 1$. Figure 6(b) shows the corresponding pitching moment coefficient $M_y/\alpha$ vs $H_0$ for the case. $M_y$ is in the direction of the pitching and $M_y/\alpha$ increases with the proximity of the body to the ground and also with the angle of attack.

To explain these trends to the angle of attack, we calculated the distribution of the differential vertical force $dF_z = f_z/(\rho_f U^2 \varepsilon^3)$ of (43b). Figure 7 shows $dF_z$ vs $x$ for the spheroid at $H_0 = 1.5$ and various angles of attack. At $\alpha = 0.0$, $dF_z$ is symmetrical about the center position $x = 0$ of the body, positive near its two ends, negative along the large middle part, and reaches its minimum at the center. As $\alpha$ increases, the increment of $dF_z$ in the fore half of the body, farther from the ground, is less than the decrement in the aft half, due to nonlinear effect, and therefore the attraction and pitching moment increase.

The positive $dF_z$ at the two ends of the body may be interpreted as follows. A body experiences the repellence

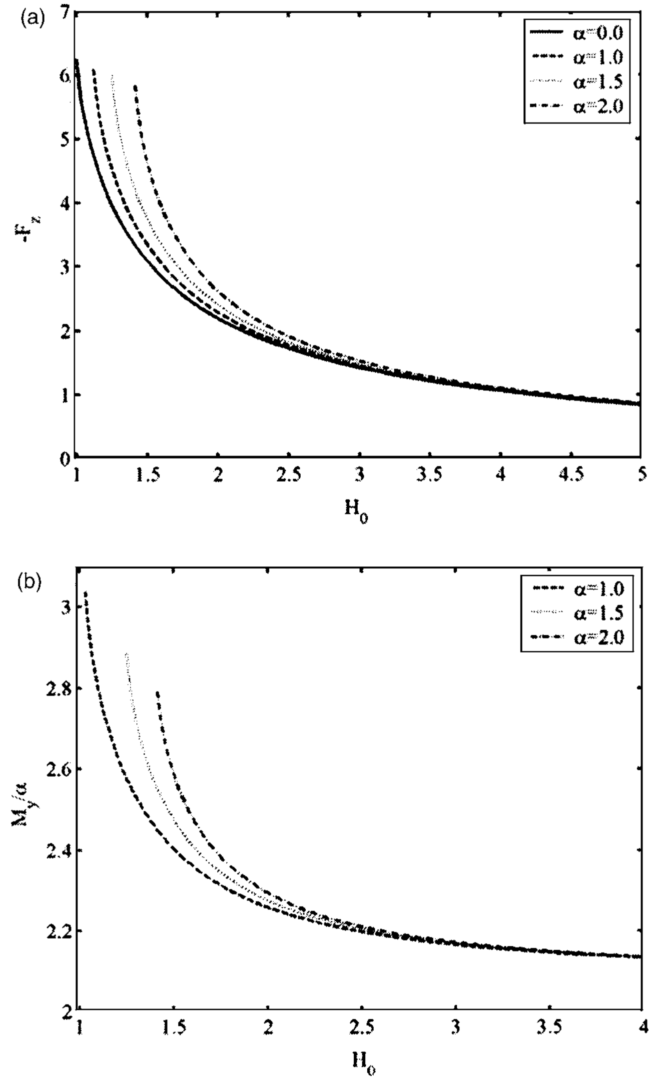


FIG. 6. (a) The attraction $-F_z$ and (b) pitching moment coefficient $M_y/\alpha$ vs the body center height $H_0$ for a slender spheroid at $\alpha$=0.0, 1.0, 1.5, and 2.0 moving over a flat ground.

when it approaches (or departs from) a wall (or another body);[2,25,26] whereas it experiences attraction when it passes by a wall (or another body).[11,12,25,27] In this case, the two ends of the spheroid appear approaching (departing from) the wall locally, therefore, $dF_z$ over there is positive.

We then compare the two slender bodies of revolution defined as

$$A(x) = (1 - 4x^2/L^2)^\gamma \quad \text{for } |x| \leqslant L/2, \tag{56}$$

at $\gamma=1/2$ (spheroid) and 1/3, moving over a flat ground. Figures 8(a) and 8(b) show the attractions $-F_z$ and pitching moment $M_y$ vs $H_0$, at $\alpha$=0.0 and 1.0. The attraction and pitching moment on the body at $\gamma=1/3$ are larger than those on the ellipsoid, and the differences are prominent when the clearance beneath the body is small, $H_0 \leqslant 1.5$. This is as expected since the clearance beneath the body at $\gamma=1/3$ is smaller. The attraction and pitching moment on the body at $\gamma=1/3$ increase with its proximity to the ground and with the angle of attack too.

We further analyze the effects of the angle of yaw $\delta$. Figures 9(a) and 9(b) show the attraction $-F_z$ and pitching moment $M_y$ vs $H_0$, for a slender spheroid in ground effect, at $\alpha$=1.0 and $\delta$=0.0, 0.5, and 1.0, respectively. When $H_0 \leqslant 1.5$, the attraction and pitching moment increase rapidly with $\delta$. As noticed in Sec. III, there is a lateral cross flow at the velocity of $U\delta$ due to yaw, which moves faster beneath the body, because of the constraining effect of the wall. When the body is very close to the wall, the imbalance of the lateral cross flow is strong and the attraction increases significantly. This flow imbalance is stronger for the aft half of the body closer to the wall at $\alpha$=1.0, hence the pitching moment increases too.

As noticed in Sec. IV B, no side force acts on a body at an angle of yaw when it is in a steady horizontal translation near a wall. Nevertheless the body experiences a yaw moment. Figure 10 shows the yaw moment coefficient $M_z/\delta$ vs $H_0$ for the body at $\delta$=1.0 and $\alpha$=0.0, 1.0, 1.5, and 2.0. The

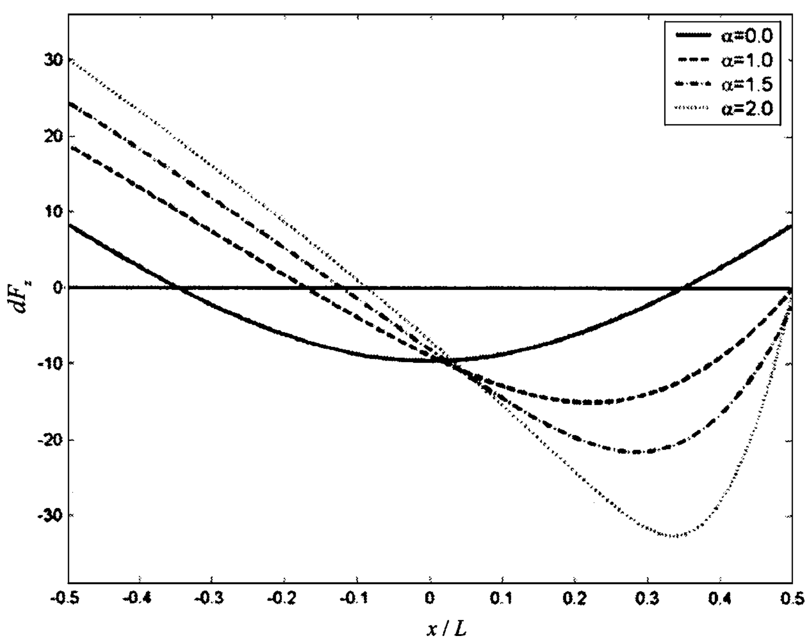


FIG. 7. The differential vertical force $dF_z$ vs $x$ on a slender spheroid at $H_0$=1.5 and various angles of attack moving over a flat ground.

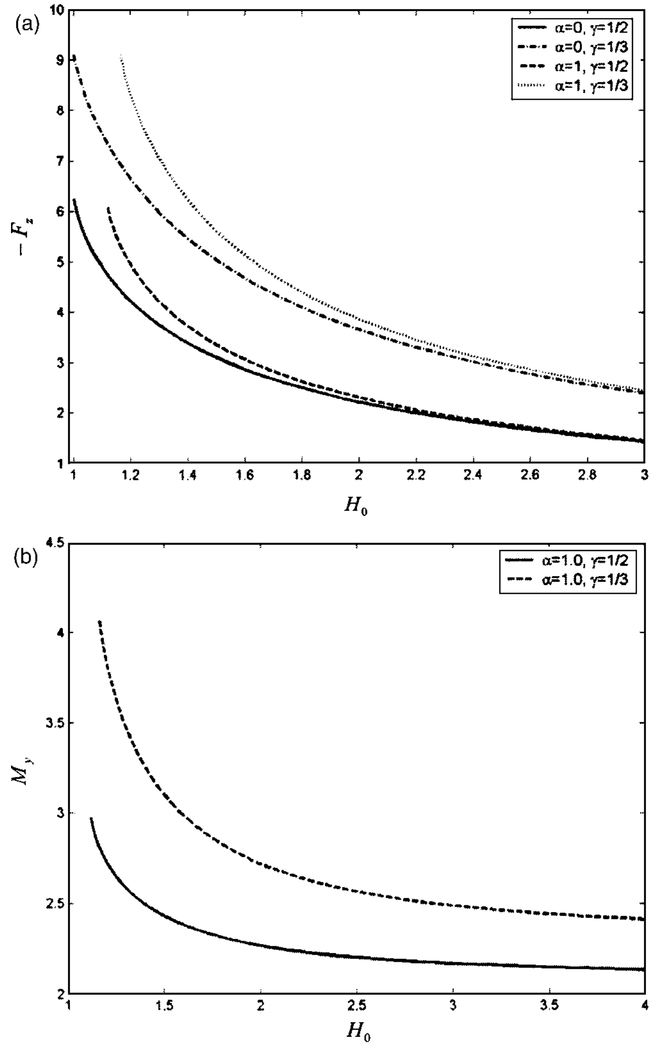


FIG. 8. (a) The attraction $F_z$ and (b) pitching moment $M_y$ vs $H_0$ for slender bodies of revolution defined by (56) at $\gamma=1/2$, $1/3$ and $\alpha=0.0$, 1.0 moving over a flat ground.

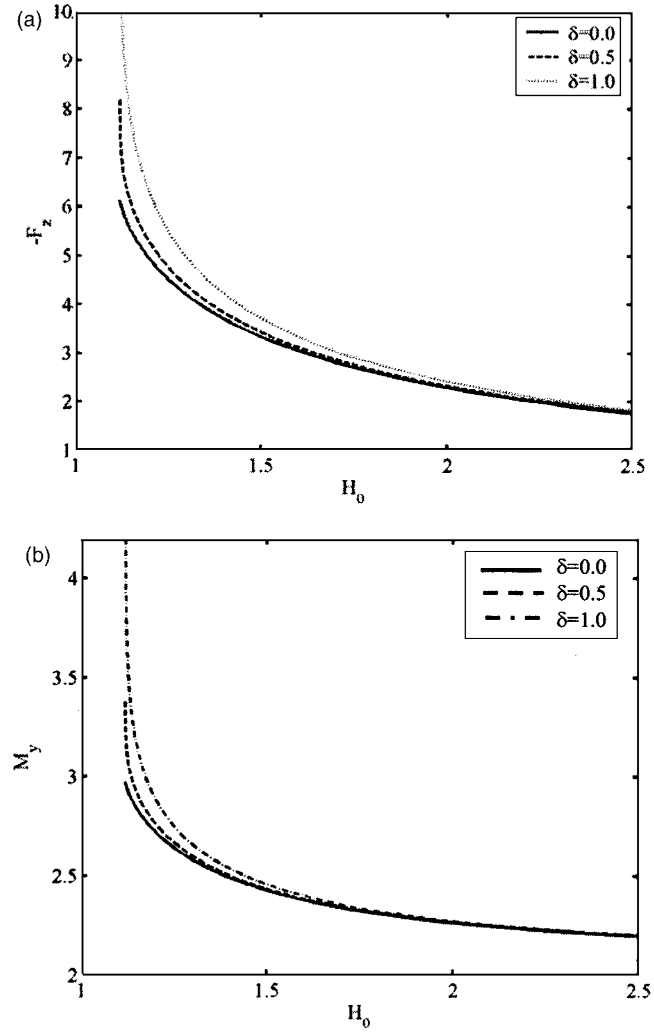


FIG. 9. (a) The attraction $-F_z$ and (b) pitching moment $M_y$ vs $H_0$ for a slender spheroid at $\alpha=1.0$ and various angles of yaw $\delta$ moving over a flat ground.

yaw moment is in the direction of the yaw and its amplitude increases with the proximity of the body to the wall and also with the angle of attack.

### B. Convex- and concave-ground effects

The curved-ground effect is a transient problem. Suppose a part of the ground is of a cylindrical quadratic profile as follows:

$$F_g(x-Ut,y)=\begin{cases} B\left(1-\dfrac{|x+L/2+\lambda-Ut|^2}{\lambda^2}\right) & \text{for } |x+L/2+\lambda-Ut| \leqslant \lambda, \\ 0 \quad \text{for } |x+L/2+\lambda-Ut| > \lambda, \end{cases} \tag{57}$$

where $B$ and $2\lambda$ are the amplitude and range of the curved part. With the definition, the nose of the body is precisely above the beginning of the curved part at time $t=0$ and its aft end is above the end of the curved part at $t=(L+2\lambda)/U$.

Figures 11(a) and 11(b) show the attraction $-F_z$ and pitching moment $M_y$ versus time $t$ when a slender spheroid at $\alpha=1.0$ and $H_0=2.0$ moves over the curved ground at $\lambda=1.0$ and $B=0.0$, $\pm 0.25$, $\pm 0.50$, and $\pm 0.75$. The magnitudes of the attraction and pitching moment increase (decrease) when the body moves over the convex (concave) ground. This is because the constraining effect of the ground on the flow beneath the body is strengthened (weakened) by a con-

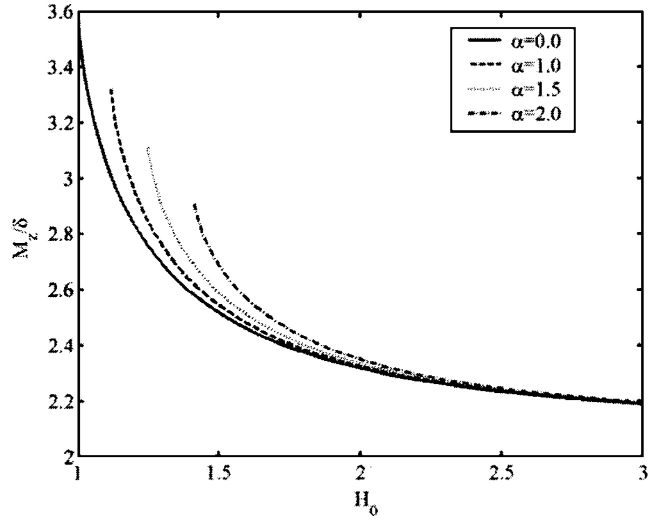


FIG. 10. The yaw moment coefficient $M_z/\delta$ vs $H_0$ for a slender spheroid at $\delta=1.0$ and $\alpha=0.0$, 1.0, 1.5, and 2.0 moving over a flat ground.

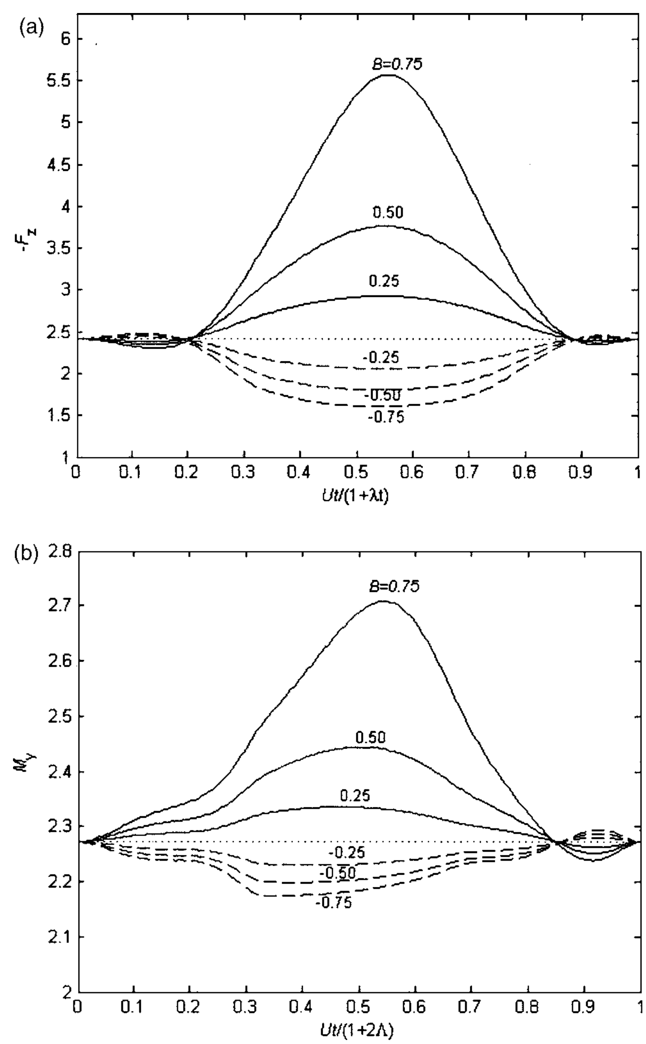


FIG. 11. (a) The attraction $-F_z$ and (b) pitching moment $M_y$ vs time for a slender spheroid at $\alpha=1.0$ and $H_0=2.0$ moving over the convex ground (solid line), flat ground (dash-dot line), and concave ground (dash line), defined by (57), at $\lambda=1.0$ and various amplitudes.

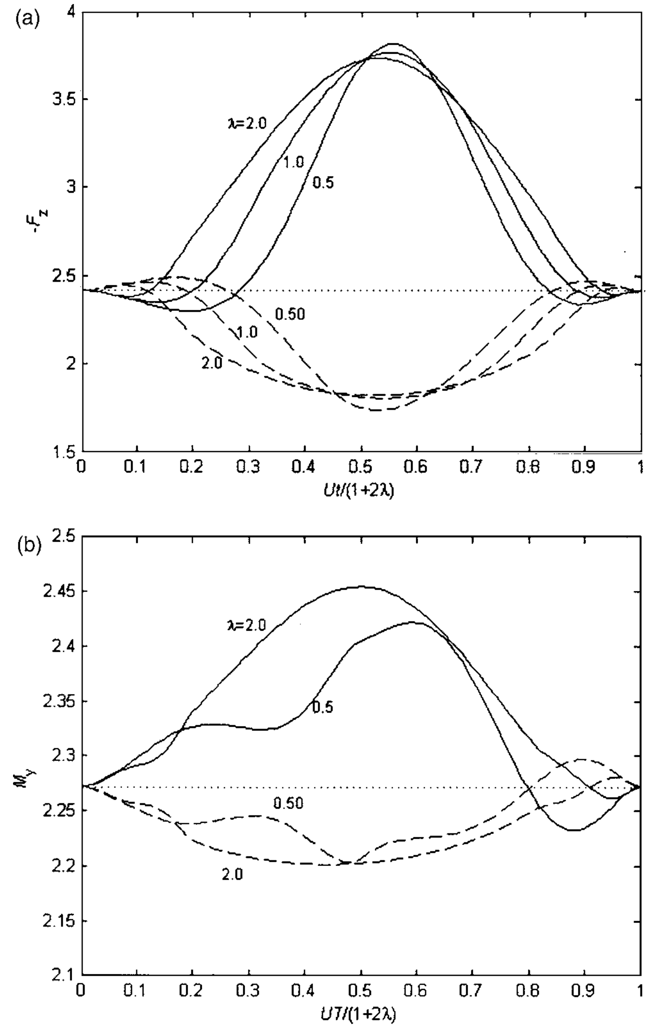


FIG. 12. (a) The attraction $-F_z$ and (b) pitching moment $M_y$ vs time for a slender spheroid at $\alpha=1.0$ and $H_0=2.0$ moving over the convex ground (solid line), flat ground (dot line), and concave ground (dash line), defined by (57), at various wavelengths.

vex (concave) ground. The variations of the attraction and pitching moment appear antisymmetrically between $B=\pm 0.25$, but become asymmetric at $B=\pm 0.50, \pm 0.75$, where the increments due to the convex ground are much larger. This is because, compared to $B=-0.5, -0.75$, the clearance beneath the body at $B=0.5, 0.75$ is much smaller.

The reverse trend for the attraction is noticed in Fig. 11(a) when a small fore part of the body enters over the curved part of the ground or a small rear part of the body leaves over the curved part. Under those situations, the attraction decreases (increases) due to the convex (concave) ground. This is because the differential vertical force near the two ends is positive as noticed in Fig. 7. The reverse trend for the pitching moment in Fig. 11(b), as a small rear part of the body leaving over the curved part, is due to the same reason.

We next consider the influence of the curvature of the curved ground. Figures 12(a) and 12(b) show the attraction $-F_z$ and pitching moment $M_y$ versus time when the spheroid at $\alpha=1.0$ and $H_0=2.0$ moves over the convex ground (solid line, $B=0.5$), flat ground (dot line), and concave ground

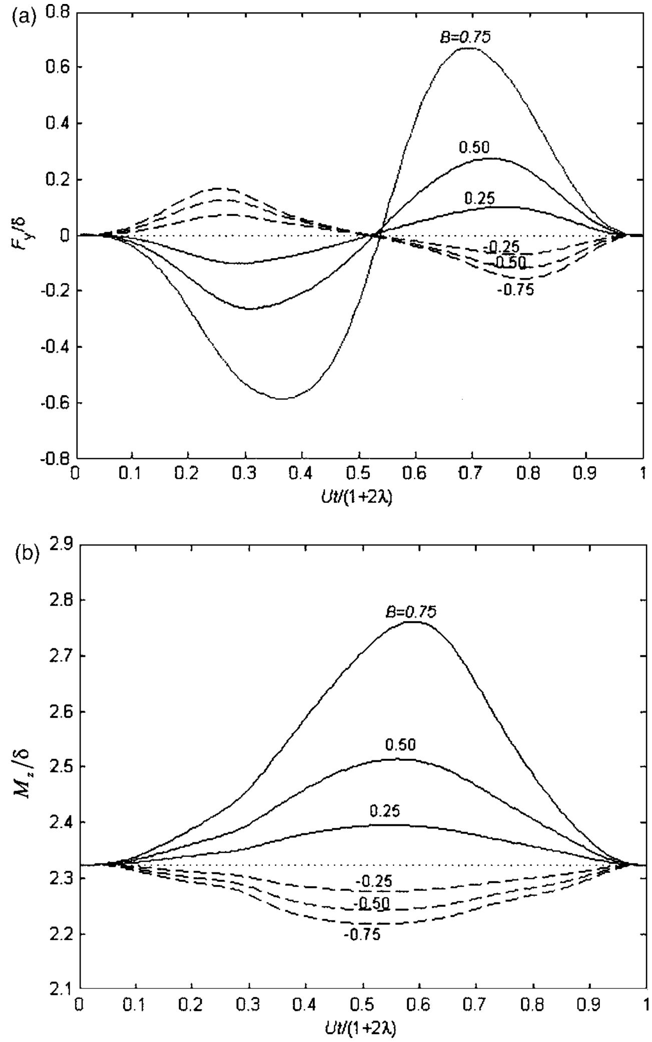


FIG. 13. (a) The side force coefficient $F_y/\delta$ and (b) yaw moment coefficient $M_z/\delta$ vs time for a slender spheroid at $\alpha=1.0$, $\delta=1.0$, and $H_0=2.0$ moving over the convex ground (solid line), flat ground (dot line), and concave ground (dash line), defined by (57), at $\lambda=1.0$ and various amplitudes.

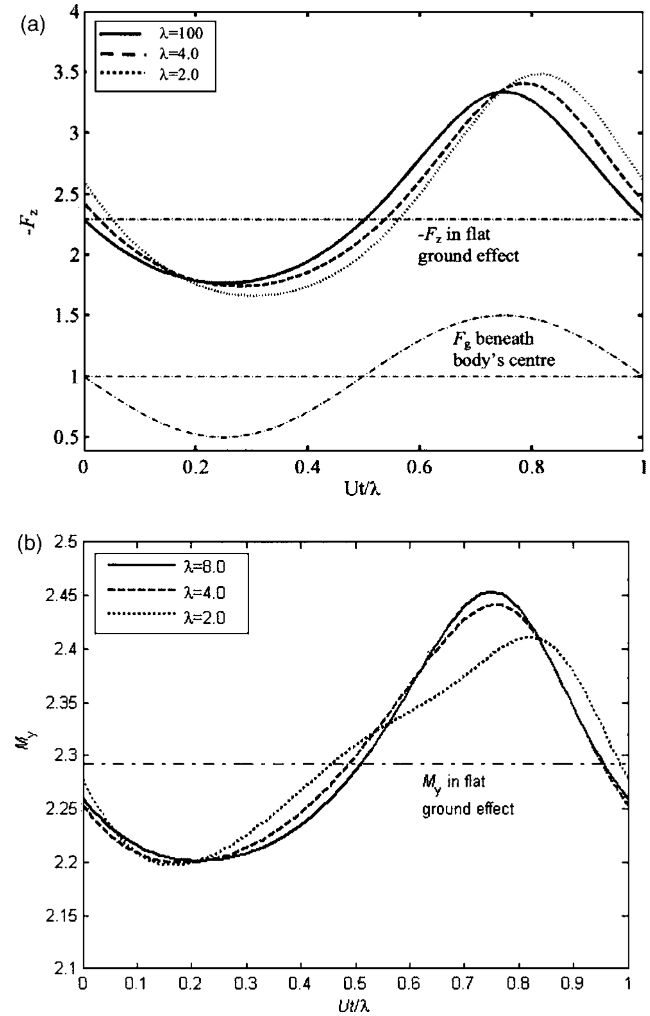


FIG. 14. (a) The attraction $-F_z$ and (b) pitching moment $M_y$ vs time for a slender spheroid at $\alpha=1.0$ and $H_0=2.0$ moving over the wavy ground at amplitude $B=0.5$ and various wavelengths.

(dash line, $B=-0.5$) at $\lambda=0.5$, 1.0 and 2.0, respectively. The variation in amplitude of the attraction increases slightly with the ground curvature, whereas the variation in amplitude of the pitching moment decreases slightly with the ground curvature.

If the body is at an angle of yaw, a side force is generated by the coupling of the lateral cross flow due to yaw and the unsteady effect due to ground curvature. Figure 13(a) shows the side force coefficient $F_y/\delta$ versus time when the body at $\alpha=1.0$, $\delta=1.0$ and $H_0=2.0$ moves over the curved ground at $\lambda=1.0$ and $B=0.0$, $\pm0.25$, $\pm0.50$, and $\pm0.75$. $F_y/\delta$ is negative as the body moves over the rising part (in the direction of the body motion) of the curved ground and vice versa. Its magnitude increases with the slope of the curved ground and also with the proximity of the body to the ground. Figure 13(b) shows the corresponding yaw moment coefficient $M_z/\delta$ versus time. $M_z/\delta$ increases (decreases) when the body moves over the convex (concave) ground. The variation amplitudes of $F_y/\delta$ and $M_z/\delta$ for the convex ground at $B=0.5, 0.75$ are much larger than those for the corresponding concave ground too.

In conclusion, the attraction, pitching moment, and yaw moment depend largely on the clearance beneath the body, and increase (decrease) when the body is over the convex (concave) ground. However, the side force depends largely on and increases with the slope of the curved ground.

### C. Wavy-ground effect

We further consider the case where a slender spheroid moving over a wavy ground

$$F_g(x-Ut,y)=B\sin[2\pi(x-Ut)/\lambda], \tag{58}$$

where $B$ and $\lambda$ are its wave amplitude and wavelength. The force and moment on the body are oscillating functions at the oscillation period of $\lambda/U$.

We first consider the variations of the force and moment versus time. Figures 14(a) and 14(b) show the attraction $-F_z$ and pitching moment $M_y$ versus time when the body at $\alpha=1.0$ and $H_0=2.0$ moves over the wavy ground at $B=0.5$ and various wavelengths. For comparison, we depict the corresponding values of $-F_z$ and $M_y$ for the body over the flat ground at the mean surface of the wavy ground (dash-dot line). We also depict the wavy-ground height beneath the

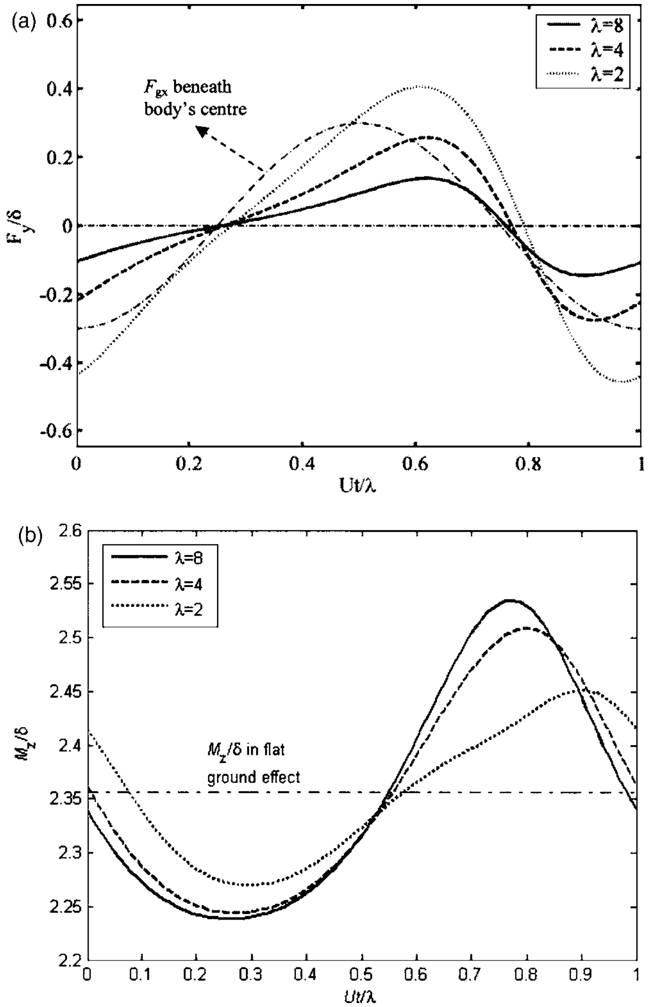


FIG. 15. (a) The side force coefficient $F_y/\delta$ and (b) yaw moment coefficient $M_z/\delta$ vs time for a slender spheroid at $\alpha=1.0$, $\delta=1.0$, and $H_0=2.0$ moving over the wavy ground at amplitude $B=0.5$ and various wavelengths.

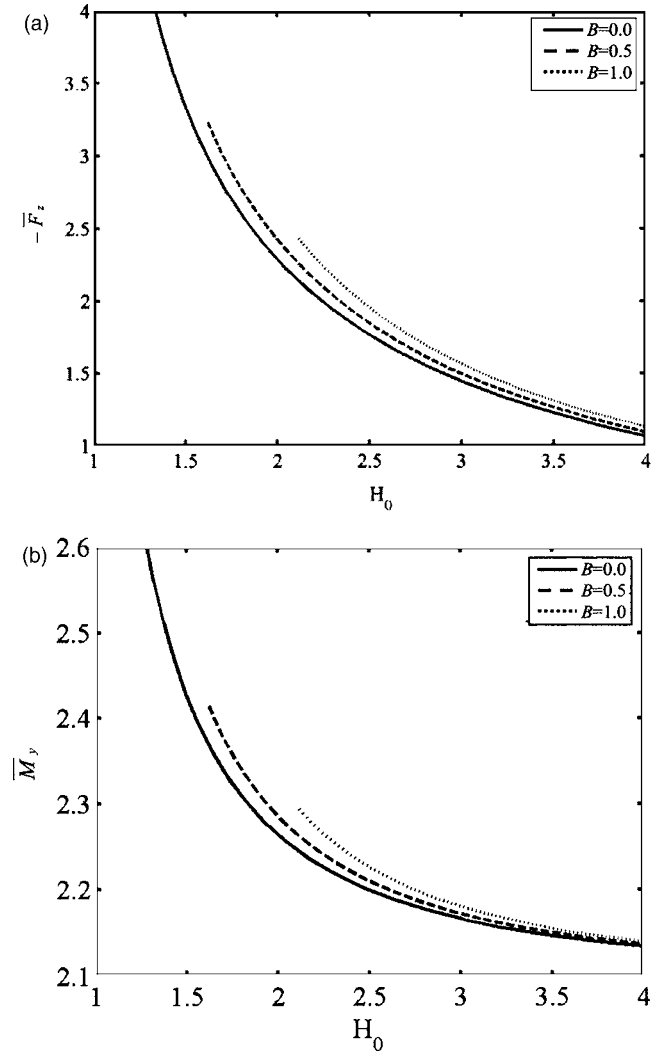


FIG. 16. (a) The mean attraction $-\bar{F}_z$ and (b) mean pitching moment $\bar{M}_y$ vs $H_0$ for a slender spheroid at $\alpha=1.0$ moving over the wavy ground at amplitudes $B=0.0$ (flat ground), 0.5, and 1.0.

body center versus time. The attraction and pitching moment are roughly in phase with the wave height beneath the body center. This is because both the attraction and pitching moment increase with the proximity of the body to the ground. The clearance between them is out of the phase with the wave height, i.e., the clearance appears the smallest (largest) when its center is over the peak (trough) of the wavy ground. When the wavelength is comparable to the body length, at $\lambda=4$ and 2, the phase of $-F_z$ is slightly behind that of the wave height. This is because, at $\alpha=1.0$, the aft half of the body closer to the ground has more contributions to $-F_z$. The variation in amplitude of $-F_z$ and $M_y$ is much larger when the body center is over the upper half of the wavy ground than that over the low half.

Figures 15(a) and 15(b) show the side force coefficient $F_y/\delta$ and yaw moment coefficient $M_z/\delta$ versus time when the body at $\alpha=1.0$, $\delta=1.0$, and $H_0=2.0$ moves over the wavy ground at $B=0.5$ and various wavelengths. For comparison, we also depict the slope of the wavy ground beneath the body center versus time. $F_y/\delta$ is roughly in phase with the slope of the wavy ground. $M_z/\delta$ appears in phase with the wave height beneath the body center.

In conclusion, the attraction, pitching moment, and yaw moment on the body are roughly in phase with the wave height beneath the body center because they depend largely on the clearance beneath the body, as noticed in Sec. V B. However, the side force is roughly in phase with the slope of the wavy ground. This is because the side force is generated by the coupling of the lateral cross flow due to yaw and the unsteady effect due to ground curvature, and depends largely on the slope of the curved ground.

We then consider the mean values of the oscillating force and moment. It can be verified using (36), (40), and (44)–(48) that their mean values do not vary with the wavelength of the wavy ground. Figures 16(a) and 16(b) show the mean attraction $-\bar{F}_z$ and mean pitching moment $\bar{M}_y$ vs $H_0$ when the spheroid at $\alpha=1.0$ moves over the wavy ground at $B=0.0$ (flat ground), 0.5, and 1.0. Both $-\bar{F}_z$ and $\bar{M}_y$ increase with the wave amplitude and also with the proximity of the body to the ground. This is because of the dynamic asymmetry between the body over the upper and lower halves of the wavy ground, as noticed in Fig. 14. Figures 17(a) and 17(b)

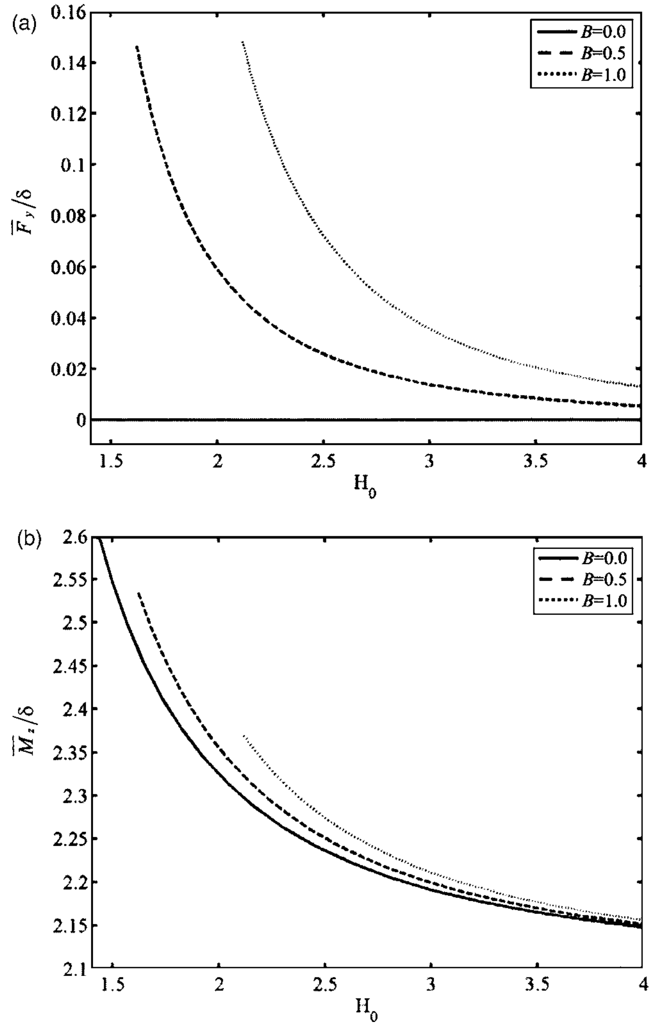


FIG. 17. (a) The mean side force coefficient $\bar{F}_y/\delta$ and (b) mean yaw moment coefficient $\bar{M}_z/\delta$ vs $H_0$ for a slender spheroid at $\alpha=1.0$ and $\delta=1.0$ moving over the wavy ground at amplitudes $B=0.0$ (flat ground), 0.5, and 1.0.

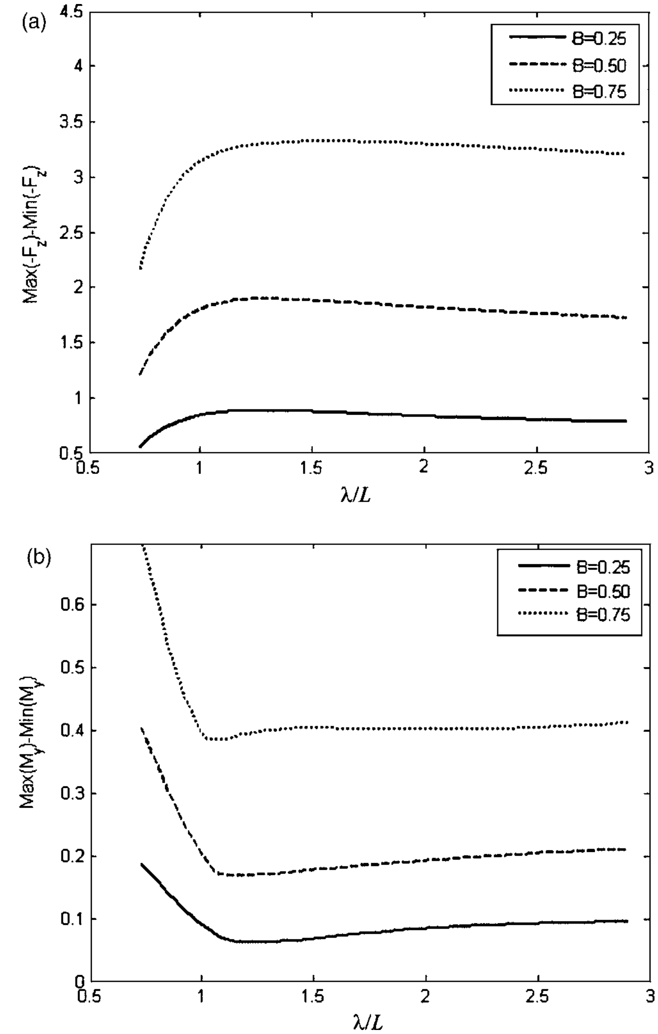


FIG. 18. The peak to trough variations of (a) the attraction $-F_z$ and (b) pitching moment $M_y$, vs the wavelength, for a slender spheroid at $\alpha=1.0$ and $H_0=2.0$ moving over the wavy ground at amplitudes $B=0.25$, 0.50, and 0.75, respectively.

show the mean side force coefficient $\bar{F}_y/\delta$ and mean yaw moment coefficient $\bar{M}_z/\delta$ vs $H_0$, as the body is at $\alpha=1.0$ and $\delta=1.0$. They both increase with the wave amplitude and with the proximity of the body to the ground too.

At last, we consider the peak to trough variations of the force and moment, which are the difference between the maximum and minimum values of the oscillating functions. Figures 18(a) and 18(b) show the peak to trough variations of the attraction $-F_z$ and pitching moment $M_y$ versus the wavelength when the spheroid at $\alpha=1.0$ and $H_0=2.0$ moves over the wavy ground at $B=0.25$, 0.50, and 0.75, respectively. The variation amplitude of the attraction first increases with the wavelength, reaches its maximum in the range of $\lambda/L=1.0-1.5$, and then decreases slowly. In contrast, the variation amplitude of the pitching moment first decreases rapidly with the wavelength, reaches its minimum around $\lambda/L\approx 1.0$, and increases slowly after that [Fig. 18(b)].

The above variation trends can be interpreted by examining the clearance distribution beneath the body. As an illustration, we discuss the attraction versus the wavelength for the case of $\lambda<L$. The attraction reaches its peak (trough) when the body center is over the peak (trough) of the wavy ground [Fig. 14(a)]. Figures 19(a) and 19(b) show the clear-

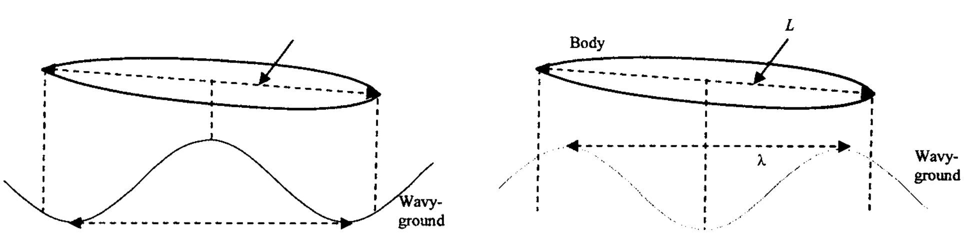


FIG. 19. A slender body moving over (a) the peak and (b) trough of a wavy ground for $\lambda<L$.

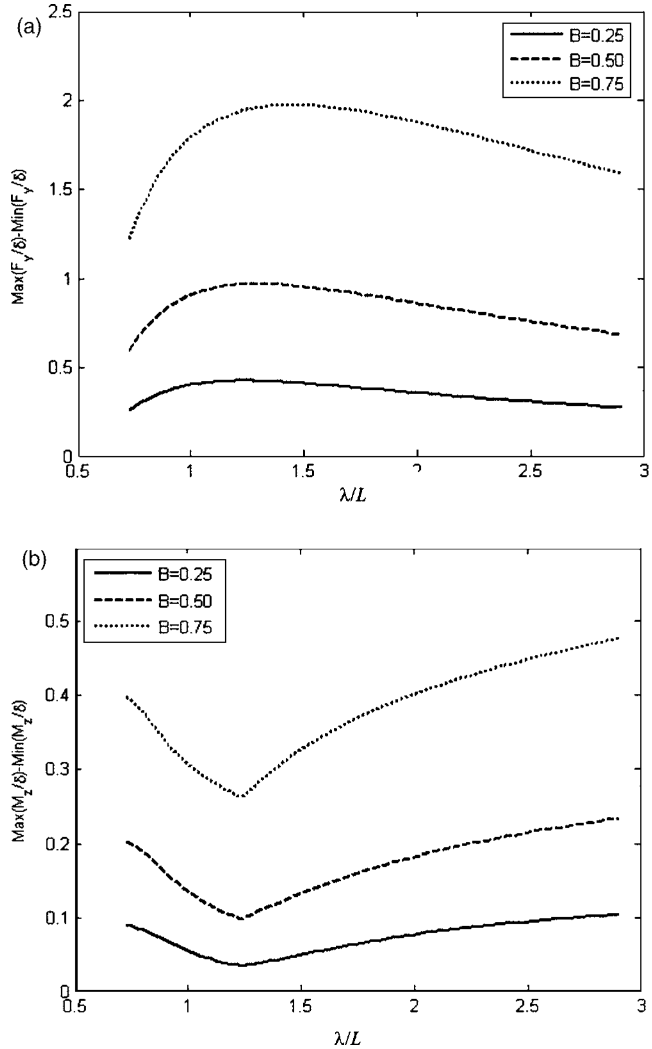


FIG. 20. The peak to trough variations of (a) the side force coefficient $F_y/\delta$ and (b) yaw moment coefficient $M_z/\delta$ vs the wavelength, for a slender spheroid at $\alpha=1.0$, $\delta=1.0$, and $H_0=2.0$, moving over the wavy ground at amplitudes $B=0.25$, 0.50, and 0.75, respectively.

ance distribution beneath the body as the body center over the peak and trough of a wavy ground at $\lambda < L$. As the body center over the peak of the wavy ground [Fig. 19(a)], if the wavelength increases, the clearance decreases beneath the middle part of the body and increases near its two ends. Because the middle part of the body experiences the attraction and its two ends experiences repellence (Fig. 7), the peak of the attraction thus increases. As the body center over the trough of the wavy ground [Fig. 19(b)], if the wavelength increases, the clearance increases beneath the middle part of the body and decreases near its two ends, hence the trough of the attraction decreases. Consequently the peak to trough variation of the attraction $-F_z$ increases with the wavelength as $\lambda < L$. Similar interpretations are suitable for the case of $\lambda > L$ as well as for the pitching moment.

Figures 20(a) and 20(b) show the peak to trough variations of the side force coefficient $F_y/\delta$ and yaw moment coefficient $M_z/\delta$ versus the wavelength when the body at $\alpha=1.0$, $\delta=1.0$, and $H_0=2.0$ moves over the wavy ground. The variation amplitude of $F_y/\delta$ first increases with the wavelength, reaches its maximum in the range of $\lambda/L=1.0-1.5$, and then decreases slowly. In contrast, the variation amplitude of $M_z/\delta$ first decreases with the wavelength, reaches its minimum around $\lambda/L \approx 1.25$, and increases after that.

## VI. SUMMARY AND CONCLUSIONS

The irrotational flow induced by a slender body in a horizontal translation over a curved ground was analyzed by extending the classical slender body theory. Like a slender body in an unbounded field, the flow far away from the body was shown to be a direct problem, represented by the line source distribution along the body length, but at the double strength. The flow near the body was reduced to the two-dimensional flow problem of the deformation, the vertical and lateral translations of double cylinders, in a symmetrical manner. The unsteady effect of the ground curvature depends only on the ground undulation along the body length.

An analytical flow solution was obtained for a slender body of revolution at angles of attack and yaw, moving over an arbitrary curved ground. The attraction and side force, and pitching and yaw moments, were obtained in the form of the integrals along the body length. Numerical analyses were carried out for the body in curved-ground effect. Some irrotational dynamic features were noticed as follows.

(1) The body experiences an attraction and a pitching moment in the direction of the pitching, when it moves near ground, and their magnitudes increase with the angle of attack and also with its proximity to the ground.
(2) When the body is at an angle of yaw, it experiences a yaw moment in the direction of yaw, and a side force too if the ground is curved. The side force coefficient $F_y/\delta$ is negative as the body moves over the rising part (in the direction of the body motion) of the curved ground and vice versa. The side force and yaw moment are proportional to the angle of yaw, whereas the attraction and pitching moment are proportional to the square of the angle of yaw.
(3) The attraction and side force are at the order of $\varepsilon^3\rho_f U^2 L^2$ and pitching and yaw moments are at the order of $\varepsilon^3\rho_f U^2 L^3$, where $\varepsilon$ is the ratio of the maximum radius of the cross section of the body to the length of the body.
(4) The ground effect is prominent when the minimum clearance beneath the body is within the body radius, and is small if the clearance is larger than twice of the diameter. The ground effect is strengthened (weakened) by a convex (concave) ground. The variations of the force and moment due to a convex ground can be significantly larger than that due to the concave ground at the same amplitude.
(5) In the wavy-ground effect, the attraction and pitching and yaw moments appear in phase with the wave height beneath the body center, but the side force appears in phase with the wave slope beneath the body center. The nonlinear/unsteady effects are significant when the wavelength is comparable to the body length and/or the wave amplitude is comparable to the clearance between them. The mean force and moment components increase

with the wave amplitude. The variation in amplitude of attraction and side force first increases with the wavelength, reaches their maximums in the range of $\lambda/L=1.0-1.5$, and then decreases slowly. In contrast the variation in amplitude of the pitching and yaw moments first decreases with the wavelength, reaches their minimums in the range of $\lambda/L=1.0-1.5$, and increases after that.

## ACKNOWLEDGMENTS

This work was partially carried out when the author studied at the University of Science and Technology of China under the guidance of Professor L. X. Zhuang and Professor B. G. Tong. This work was partially funded by the Maritime and Port Authority of Singapore.

## APPENDIX A: THE DERIVATION OF (31)

Although formulas (31) of the force and moment on a body in a potential flow are standard (cf. Ref. 28, Chap. 4), they play a crucial role in this paper, which are derived briefly in this appendix. Using the Bernoulli equation, the force $\boldsymbol{f}$ and moment $\boldsymbol{m}_0$ on the body are

$$\frac{\boldsymbol{f}}{\rho_f} = -\int_{S_c}\left(\frac{\partial\varphi}{\partial t}\varphi_n + \frac{1}{2}\nabla\varphi\cdot\nabla\varphi\right)\boldsymbol{n}dS, \tag{A1a}$$

$$\frac{\boldsymbol{m}_0}{\rho_f} = -\int_{S_c}\left(\frac{\partial\varphi}{\partial t}\varphi_n + \frac{1}{2}\nabla\varphi\cdot\nabla\varphi\right)(\boldsymbol{R}_0\times\boldsymbol{n})dS, \tag{A1b}$$

where $S_b$ is the body surface and $S_c$ a fixed control surface exterior to $S_b$, as shown in Fig. 3.

On the fixed control surface $S_c$,

$$\frac{d}{dt}\int_{S_c}\varphi\boldsymbol{n}dS = \int_{S_c}\frac{\partial\varphi}{\partial t}\boldsymbol{n}dS. \tag{A2}$$

Using the Gauss theorem and then the transport theorem,

$$\begin{aligned}\frac{d}{dt}\int_{S_c+S_b}\varphi\boldsymbol{n}dS &= \frac{d}{dt}\int_{V(t)}\nabla\varphi dV\\ &= \int_{V(t)}\nabla\left(\frac{\partial\varphi}{\partial t}\right)dV + \int_{S_c+S_b}\nabla\varphi v_n dS\\ &= \int_{S_c+S_b}\left(\frac{\partial\varphi}{\partial t}\boldsymbol{n} + \nabla\varphi v_n\right)dS\\ &= \int_{S_b}\left(\frac{\partial\varphi}{\partial t}\boldsymbol{n} + \frac{\partial\varphi}{\partial n}\nabla\varphi\right)dS + \int_{S_c}\frac{\partial\varphi}{\partial t}\boldsymbol{n}dS,\end{aligned} \tag{A3}$$

where $V(t)$ is the control volume surrounded by $S_b$ and $S_c$. $\nu_n$ is the normal velocity on the surfaces, being zero on $S_c$ and equaling $\varphi_n$ on $S_b$.

Subtracting (A2) from (A3),

$$\frac{d}{dt}\int_{S_b}\varphi\boldsymbol{n}dS = \int_{S_b}\left(\frac{\partial\varphi}{\partial t}\boldsymbol{n} + \frac{\partial\varphi}{\partial n}\nabla\varphi\right)dS. \tag{A4}$$

Adding (A4) to (A1),

$$\frac{\boldsymbol{f}}{\rho_f} = -\frac{d}{dt}\int_{S_b}\varphi\boldsymbol{n}dS + \int_{S_b}\left(\varphi_n\nabla\varphi - \boldsymbol{n}\frac{1}{2}\nabla\varphi\cdot\nabla\varphi\right)dS. \tag{A5}$$

Using the Gauss theorem,

$$\begin{aligned}&\int_{S_b+S_c}\left(\varphi_n\nabla\varphi - \boldsymbol{n}\frac{1}{2}\nabla\varphi\cdot\nabla\varphi\right)dS\\ &\quad= \int_{V(t)}\left[\frac{\partial}{\partial x_j}\left(\frac{\partial\varphi}{\partial x_j}\nabla\varphi\right) - \frac{1}{2}\nabla(\nabla\varphi\cdot\nabla\varphi)\right]dV\\ &\quad= \int_{V(t)}\nabla\varphi\Delta\varphi dV = 0.\end{aligned} \tag{A6}$$

It follows that the second integral in (A5) may be replaced by the negative of the same integral over $S_c$ to give the desired expression of (31a).

Similarly, the relation

$$\int\nabla\times\boldsymbol{Q}dV = \int(\boldsymbol{n}\times\boldsymbol{Q})dS \tag{A7}$$

can be used to derive from (A1b) an alternative expression for the moment as given in (31b).

## APPENDIX B: THE DERIVATION OF (44)

To calculate the three integrals in (44) along $C_1$ and $C_g$ in the cross-flow plane $T$, we transform them to that along the corresponding circles $B_1$ and $B_0$ in the mapped plane $\varsigma$,

$$I_1(x,t) = \oint_{C_1}\phi\cos\theta\, dl = \oint_{B_1}\phi\cos\theta J\, dl, \tag{B1}$$

$$J_1(x,t) = \oint_{C_1}\phi\sin\theta\, dl = \oint_{B_1}\phi\sin\theta J\, dl, \tag{B2}$$

$$J_2(x,t) = \frac{1}{2}\oint_{C_g}(\phi_Y^2 + \phi_Z^2)dl = \frac{1}{2}\oint_{B_0}\left(\phi_\rho^2 + \frac{1}{\rho^2}\phi_\Theta^2\right)J^{-1}dl, \tag{B3}$$

where $J=|dT/d\varsigma|$. Using (21)–(23), (26), and (27), one can obtain $J\cos\theta$ and $J\sin\theta$ on $B_1$ and $J$ on $B_0$,

$$(J\cos\theta)|_{B_1} = f_2(\Theta) = \frac{2}{e^\beta}\sum_{n=1}^{\infty}n\frac{\sin(n\Theta)}{e^{n\beta}}, \tag{B4}$$

$$(J\sin\theta)|_{B_1} = -f_1(\Theta) = \frac{2}{e^\beta}\sum_{n=1}^{\infty}n\frac{\cos(n\Theta)}{e^{n\beta}}, \tag{B5}$$

$$J|_{B_0} = \frac{1}{1-\cos\Theta}. \tag{B6}$$

To calculate $I_1$ and $J_1$, we expand $\phi|_{B_1}$ in terms of the Fourier series in $\Theta$

$$\phi|_{B_1} = A_0 + 2\sum_{n=1}^{\infty} \frac{1}{n}[A_n \cos(n\Theta) + B_n \sin(n\Theta)], \tag{B7}$$

where

$$\begin{aligned} &A_0 = -F \ln \rho_1, \quad A_n = [F + nCU\alpha \coth(n\beta)]e^{-n\beta}, \\ &B_n = -nCU\delta \coth(n\beta)e^{-n\beta}. \end{aligned} \tag{B8}$$

Substituting (B4) and (B7) into (B1), we have

$$\begin{aligned} I_1(x,t) &= 2C\int_0^{2\pi} \left[ \sum_{n=1}^{\infty} n\frac{\sin(n\Theta)}{e^{n\beta}} \right] \\ &\quad \times \left\{ A_0 + 2\sum_{n=1}^{\infty} \frac{1}{n}[A_n \cos(n\Theta) + B_n \sin(n\Theta)] \right\} d\Theta \\ &= 4\pi C\sum_{n=1}^{\infty} (B_n e^{-n\beta}) \\ &= -4\pi C^2 U\delta\sum_{n=1}^{\infty} [n \coth(n\beta)e^{-2n\beta}]. \end{aligned} \tag{B9}$$

In the above equation, we have used the following integral formulas

$$\begin{aligned} &\int_0^{2\pi} \sin(n\Theta)\cos(m\Theta)d\Theta = 0, \\ &\int_0^{2\pi} \sin(n\Theta)\sin(m\Theta)d\Theta = \pi\delta_{nm} \quad \text{for } n,m \geqslant 1, \end{aligned} \tag{B10}$$

where $\delta_{nm}$ is the Kronecker delta, i.e., $\delta_{nm}=0$ as $n \neq m$ and $\delta_{nm}=1$ as $n=m$.

Similarly substituting (B5) and (B7) into (B2), we have

$$\begin{aligned} J_1(x,t) &= 2C\int_0^{2\pi} \left[ \sum_{n=1}^{\infty} n\frac{\cos(n\Theta)}{e^{n\beta}} \right] \\ &\quad \times \left\{ A_0 + 2\sum_{n=1}^{\infty} \frac{1}{n}[A_n \cos(n\Theta) + B_n \sin(n\Theta)] \right\} d\Theta \\ &= 4\pi C\sum_{n=1}^{\infty} (A_n e^{-n\beta}) \\ &= 2\pi F(H-C) + 4\pi C^2 U\alpha\sum_{n=1}^{\infty} [n \coth(n\beta)e^{-2n\beta}]. \end{aligned} \tag{B11}$$

To calculate $J_2$, we need $\phi_\rho$ and $\phi_\Theta$ on $B_0$. Noticing the normal derivative of $\phi$ is zero on $C_g$ in the cross-flow plane $T$, we have

$$\phi_\rho|_{B_0} = 0. \tag{B12}$$

We further expand $\phi_\Theta$ on $B_0$ in terms of the Fourier series in $\Theta$ using (30)

$$\begin{aligned} \phi_\Theta|_{B_0} &= -F\frac{\sin \Theta}{1-\cos \Theta} + 2\sum_{n=1}^{\infty} C_n \sin(n\Theta) \\ &\quad + 2\sum_{n=1}^{\infty} D_n \cos(n\Theta), \end{aligned} \tag{B13}$$

where

$$C_n = -CU\alpha c_n, \quad D_n = -CU\delta c_n, \tag{B14}$$

and $c_n$ is given in (45).

Substituting (B6), (B12), and (B13)–(B14) into (B3), one can obtain

$$\begin{aligned} J_2(x,t) &= \frac{1}{2C}\int_0^{2\pi} (1-\cos \Theta)\phi_\Theta^2|_{B_0} d\Theta \\ &= \frac{1}{2C}\int_0^{2\pi} \left[ F^2\frac{\sin^2 \Theta}{1-\cos \Theta} - 4F \sin \Theta\sum_{n=1}^{\infty} C_n \sin(n\Theta) + 4(1-\cos \Theta)\left[ \sum_{n=1}^{\infty} C_n \sin(n\Theta) \right]^2 \right. \\ &\quad \left. + 4(1-\cos \Theta)\left[ \sum_{n=1}^{\infty} D_n \cos(n\Theta) \right]^2 \right] d\Theta \\ &= \frac{1}{2C}\int_0^{2\pi} \left[ F^2\frac{\sin^2 \Theta}{1-\cos \Theta} - 4F \sin \Theta\sum_{n=1}^{\infty} C_n \sin(n\Theta) \right. \\ &\quad + 2(1-\cos \Theta)\left( \sum_{n=1}^{\infty}\sum_{m=1}^{\infty} C_n C_m\{\cos[(n-m)\Theta] - \cos[(n+m)\Theta]\} \right) \\ &\quad \left. + 2(1-\cos \Theta)\left( \sum_{n=1}^{\infty}\sum_{m=1}^{\infty} D_n D_m\{\cos[(n-m)\Theta] + \cos[(n+m)\Theta]\} \right) \right] d\Theta \end{aligned}$$

$$= \frac{\pi}{C}\left[ F^2 + 2AFU\alpha e^{-\beta} + 2C^2U^2(\alpha^2+\delta^2)\sum_{n=1}^{\infty} c_n(c_n - c_{n+1}) \right]. \tag{B15}$$

(B10) as well as the following integral formulas have been used in the above equation

$$\int_0^{2\pi} \cos\Theta \cos[(n+m)\Theta] d\Theta = 0, \tag{B16a}$$

$$\int_0^{2\pi} \cos\Theta \cos[(n-m)\Theta] d\Theta = \begin{cases} 0 & \text{as} |n-m| \neq 1, \\ \pi & \text{as } n = m \pm 1, \end{cases} \tag{B16b}$$

for $n, m \geqslant 1$.


[1]S. E. Widnall and T. W. Barrows, "An analytic solution for two- and three-dimensional wings in ground effect," J. Fluid Mech. **41**, 769 (1970).
[2]C. S. Yih, "Fluid mechanics of colliding plates," Phys. Fluids **17**, 1936 (1974).
[3]E. O. Tuck, "A nonlinear unsteady one-dimensional theory for wings in extreme ground effect," J. Fluid Mech. **98**, 33 (1980).
[4]E. O. Tuck, "Nonlinear extreme ground effect on thin wings of arbitrary aspect ratio," J. Fluid Mech. **136**, 78 (1983).
[5]J. N. Newman, "Analysis of small-lifting-ratio lifting surfaces in ground effect," J. Fluid Mech. **117**, 305 (1982).
[6]Q. X. Wang, "Flow around an unsteady wing close to a curved ground," J. Fluid Mech. **226**, 175 (1991).
[7]E. O. Tuck, "Hydrodynamic problems of ships in restricted water," Annu. Rev. Fluid Mech. **10**, 33 (1978).
[8]K. V. Rozhdestvensky, *Aerodynamics of a Lifting System in Extreme Ground Effect* (Springer, Berlin, 2000).
[9]J. N. Newman, "The force and moment on a slender body of revolution moving near a wall," Naval Ship R&D Centre Report No. 2127, 1965.
[10]E. O. Tuck and J. N. Newman, *Proceeding of the Tenth Symposium on Naval Hydrodynamics*, Cambridge, MA (Office of Naval Research, Washington, DC, 1974) p. 35.
[11]R. W. Yeung and W. Y. Hwang, "Nearfield hydrodynamics and interactions of ships in shallow water," J. Hydronaut. **11**, 128 (1977).
[12]R. W. Yeung and W. T. Tan, "Hydrodynamic interactions of ships with fixed obstacles," J. Ship Res. **24**, 50 (1980).
[13]S. B. Cohen and R. F. Beck, "Experimental and theoretical hydrodynamic forces on a mathematical model in confined water," J. Ship Res. **27**, 75 (1983).
[14]J. A. Schetz, "Aerodynamics of high-speed trains," Annu. Rev. Fluid Mech. **33**, 371 (2001).
[15]Y. H. Im and K. S. Chang, "Unsteady aerodynamics of a wing-in-ground-effect airfoil flying over a wavy wall," J. Aircr. **37**, 690 (2000).
[16]S. H. Kwag, "Lift/drag prediction of 3-dimensional WIG moving above free surface," KSME Int. J. **15**, 384 (2001).
[17]M. M. Munk, "The aerodynamic forces on airship hulls," NACA Report No. 184, 1924.
[18]M. D. Van Dyke, "Second-order theory-axisymmetric flow," NASA Report No. R-47, 1959.
[19]M. J. Lighthill, "Note on the swimming of slender fish," J. Fluid Mech. **9**, 305 (1960).
[20]J. N. Newman and T. Y. Wu, "A generalized slender-body theory for fish-like forms," J. Fluid Mech. **57**, 673 (1973).
[21]A. Sellier, "A general and formal slender-body theory in the non-lighting case," Proc. R. Soc. London, Ser. A **453**, 1733 (1997).
[22]H. Schlichting, *Boundary-Layer Theory* (McGraw-Hill, New York, 1979).
[23]M. D. Van Dyke, *Perturbation Methods in Fluid Mechanics*, 2nd ed. (Parabolic, Stanford, CA, 1975).
[24]E. O. Tuck and M. Bentwich, "Sliding sheets: lubrication with comparable viscous and inertia forces," J. Fluid Mech. **135**, 51 (1983).
[25]Q. X. Wang, "On interaction of two circular cylinders in inviscid fluids," Phys. Fluids **16**, 4412 (2004).
[26]L. M. Milne-Thomson, *Theoretical Hydrodynamics* (MacMillan, London, 1968).
[27]F. T. Korsmeyer, C. H. Lee, and J. N. Newman, "Computation of ship interaction in restricted waters," J. Ship Res. **37**, 298 (1993).
[28]J. N. Newman, *Marine Hydrodynamics* (MIT, Cambridge, MA, 1980).